

AD-A041 016

AERONAUTICAL RESEARCH COUNCIL LONDON (ENGLAND)  
THE NUMERICAL CALCULATION OF STEADY INVISCID SUPERCRITICAL FLOW--ETC(U)  
AUG 75 P W DUCK

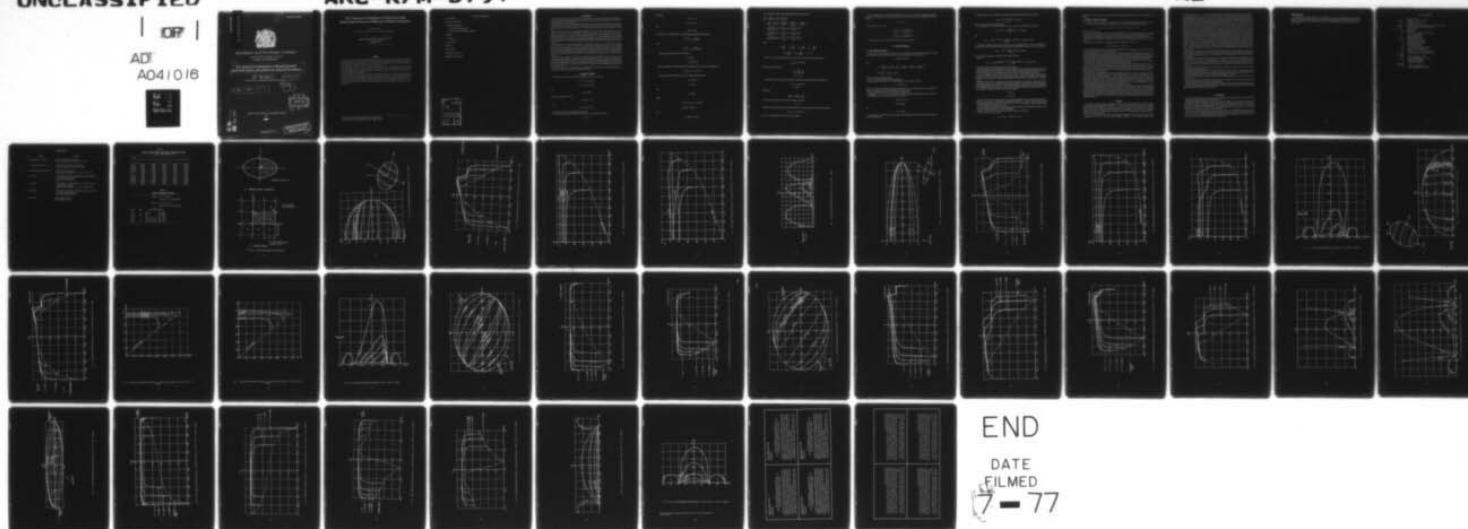
F/G 20/4

UNCLASSIFIED

ARC-R/M-3794

NL

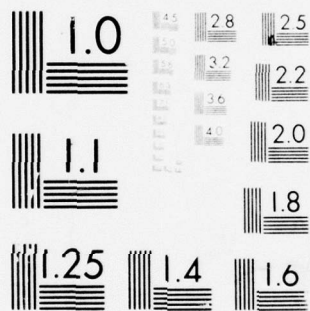
ADP  
A041 016



END

DATE  
FILMED

7-77



MICROCOPY RESOLUTION TEST CHART  
NATIONAL BUREAU OF STANDARDS-1963-A

R. & M. No. 3794

AD A 041016

R. & M. No. 3794 ✓



PROCUREMENT EXECUTIVE MINISTRY OF DEFENCE

AERONAUTICAL RESEARCH COUNCIL ✓

REPORTS AND MEMORANDA

⑥ The Numerical Calculation of Steady Inviscid  
Supercritical Flow past Ellipsoids without Circulation

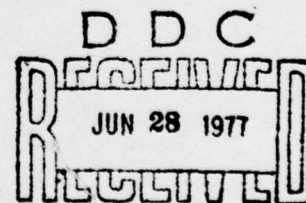
⑩ By P. W. DUCK

Theoretical Aerodynamics Unit, University of Southampton

⑪ Aug 75

⑭ ARC-R/M-3794

⑫ 49p.



LONDON: HER MAJESTY'S STATIONERY OFFICE

1977

AD No. \_\_\_\_\_  
DDC FILE COPY

008450

DISTRIBUTION STATEMENT A  
Approved for public release;  
Distribution Unlimited

# The Numerical Calculation of Steady Inviscid Supercritical Flow past Ellipsoids without Circulation

By P. W. DUCK

Theoretical Aerodynamics Unit, University of Southampton\*

---

*Reports and Memoranda No. 3794†*

*August, 1975*

---

## Summary

The previous work of the author in which the subcritical flow past ellipsoids was calculated is extended to supercritical flows. The same ellipsoidal coordinate system is used, the body-surface boundary-condition is then applied exactly (in the numerical sense). By means of a transformation of one of the coordinates, the infinite flow field is brought into a finite space for the calculation.

The complete continuity equation is approximated by the usual central differencing in the elliptic (subcritical) regions, whilst in the hyperbolic (supercritical) regions, the combination of central and non-central differencing as suggested by Albane and Jameson is used, in order to model the absence of upstream propagation of disturbances.

Although shock waves appear in the calculations, their shape and position is only approximately determined (as e.g. in transonic small perturbation theory) since the difference scheme only ensures continuity of the potential across the shock, the Rankine-Hugoniot equations not being satisfied. A number of results is presented, for flows aligned along the major and second axes, and also yawed relative to these two axes.

*The work reported here was done in connection with the link between the R.A.E. and the University of Southampton.*

---

\* Now at the Department of Mathematics, Imperial College.

† Replaces R.A.E. Technical Report 75087—A.R.C. 36 304.

## LIST OF CONTENTS

1. Introduction
2. Equations of Motion
3. Numerical Techniques
  - 3.1 Finite Difference Equation
  - 3.2 Solution of Finite Difference Equation

4. Results

5. Conclusions


List of Symbols

References

Tables 1 and 2

Illustrations—Figs. 1 to 33

Detachable Abstract Cards

ACCESSION for	
NTIS	Write Section <input checked="" type="checkbox"/>
DDC	Date Section <input type="checkbox"/>
UNANNOUNCED	<input type="checkbox"/>
JUSTIFICATION	
BY	
DISTRIBUTION, AVAILABILITY CODES	
Dist.	AVAIL. and/or SPECIAL
A	

## 1. Introduction

The development of powerful electronic computers in the last few years has enabled numerical techniques to be developed to deal with the problem of transonic flow past two-dimensional aerofoil sections, and more recently past three-dimensional bodies.

Magnus and Yoshihara<sup>1</sup> overcame the difficulty of the presence of both subcritical and supercritical regions within the flow, by considering the steady-state solution to be the limit of a non-steady solution, and thereby ensured a fully hyperbolic system, at the expense of introducing into the problem a further dimension, namely time.

Murman and Cole<sup>2</sup> introduced the mixed finite difference scheme. This approximates derivatives in elliptic regions in the usual way, by central differences, whilst in hyperbolic regions, derivatives in one of the coordinate directions (the one most closely aligned with the flow) are approximated using backward differencing (with respect to the flow direction). Other derivatives are centrally differenced. Physically this scheme is an attempt to model the absence of upstream propagation of the flow information in the supersonic zones, disturbances at a point being transmitted solely within the downstream Mach cone which has its apex at that point.

This method was also applied successfully by Garabedian and Korn<sup>3</sup> for two-dimensional aerofoils. However if the local velocity in the supersonic region departs appreciably from one of the coordinate directions, numerical instability can occur. To overcome this problem, Albane<sup>4</sup> and Jameson<sup>5</sup> have suggested transforming the principal part of the potential equation, in hyperbolic regions, into a new coordinate system, with one axis aligned along the local flow direction. Second derivatives in the direction of the flow are then differenced backwardly, whilst other derivatives are centrally differenced. Elliptic regions are treated in the usual way.

This report is an extension of the work on subcritical flow past ellipsoids of Duck<sup>6</sup>. The flow around ellipsoids without circulation is considered (implying no trailing vortex sheets) using the full equations of motion and the ellipsoidal coordinate system, which facilitates the exact implementation of the body-surface boundary-condition. Further, by means of a simple transformation, the infinite physical flow field is brought into a finite working space. In the supersonic regions, the proportion of retarded differencing suggested in Refs. 4 and 5 is used.

Attention is restricted to local Mach numbers only slightly in excess of unity since a velocity potential is used, ignoring any changes in entropy, and any rotation in the flow.

## 2. Equations of Motion

Throughout we shall use the ellipsoidal coordinate system  $(\xi^1, \xi^2, \xi^3)$  where

$$x = [1 + (\xi^1)^2]^{\frac{1}{2}} \operatorname{dn} \xi^2 \operatorname{sn} \xi^3,$$

$$y = [\sigma + (\xi^1)^2]^{\frac{1}{2}} \operatorname{cn} \xi^2 \operatorname{cn} \xi^3$$

and

$$z = \xi^1 \operatorname{sn} \xi^2 \operatorname{dn} \xi^3,$$

where, for conciseness, we write

$$\operatorname{sn} \xi^2 \equiv \operatorname{sn}(\xi^2, \sqrt{\sigma})$$

and

$$\operatorname{sn} \xi^3 \equiv \operatorname{sn}(\xi^3, \sqrt{1-\sigma})$$

(and similarly for the other Jacobian elliptic functions).

$\sigma$  is a parameter that partly determines the ratio of axes of the ellipsoid, such that

$$0 < \sigma < 1.$$

Generally

$$0 \leq \xi^1 \leq \infty,$$

$$-2K \leq \xi^2 \leq 2K$$

and

$$-2K' \leq \xi^3 \leq 2K',$$

where  $K(K')$  is the (complementary) complete elliptic integral of the first kind, viz

$$K = \int_0^{\pi/2} \frac{d\theta}{[1 - \sigma \sin^2 \theta]^{\frac{1}{2}}}$$

and

$$K' = \int_0^{\pi/2} \frac{d\theta}{[1 - (1 - \sigma) \sin^2 \theta]^{\frac{1}{2}}}$$

It is convenient to introduce the transformation

$$\begin{aligned} \xi^1 &= \sqrt{\sigma} \operatorname{tn} \bar{\xi}^1 \\ &= \sqrt{\sigma} \operatorname{sn} \bar{\xi}^1 / \operatorname{cn} \bar{\xi}^1. \end{aligned}$$

This transformation translates the infinite physical flow field into a finite working field since

$$0 \leq \bar{\xi}^1 \leq K' \quad \text{as} \quad 0 \leq \xi^1 \leq \infty.$$

The curvilinear metrics of this new  $(\bar{\xi}^1, \xi^2, \xi^3)$  system may be written as

$$A_1 = B_2 B_3,$$

$$A_2 = B_1 B_3$$

and

$$A_3 = B_1 B_2,$$

where

$$B_1 = [\sigma \operatorname{cn}^2 \xi^2 + (1 - \sigma) \operatorname{cn}^2 \xi^3]^{\frac{1}{2}},$$

$$B_2 = [(\xi^1)^2 + \operatorname{dn}^2 \xi^3]^{\frac{1}{2}}$$

and

$$B_3 = [(\xi^1)^2 + \sigma \operatorname{sn}^2 \xi^2]^{\frac{1}{2}}.$$

The continuity equation in the transformed ellipsoidal system is now

$$\begin{aligned}
& \frac{1}{A_1^2} \left[ 1 - \frac{\Phi_1^2}{A_1^2 a^2} \right] \Phi_{11} + \frac{1}{A_2^2} \left[ 1 - \frac{\Phi_2^2}{A_2^2 a^2} \right] \Phi_{22} \\
& + \frac{1}{A_3^2} \left[ 1 - \frac{\Phi_3^2}{A_3^2 a^2} \right] \Phi_{33} - \frac{2\Phi_1\Phi_2}{A_1^2 A_2^2 a^2} \Phi_{12} - \frac{2\Phi_1\Phi_3}{A_1^2 A_3^2 a^2} \Phi_{13} - \frac{2\Phi_2\Phi_3}{A_2^2 A_3^2 a^2} \Phi_{23} \\
& + \frac{\Phi_1^2}{2A_1^4 a^2} \left[ \frac{\Phi_1}{A_1^2} \frac{\partial}{\partial \xi^1} (A_1^2) + \frac{\Phi_2}{A_2^2} \frac{\partial}{\partial \xi^2} (A_1^2) + \frac{\Phi_3}{A_3^2} \frac{\partial}{\partial \xi^3} (A_1^2) \right] \\
& + \frac{\Phi_2^2}{2A_2^4 a^2} \left[ \frac{\Phi_1}{A_1^2} \frac{\partial}{\partial \xi^1} (A_2^2) + \frac{\Phi_2}{A_2^2} \frac{\partial}{\partial \xi^2} (A_2^2) + \frac{\Phi_3}{A_3^2} \frac{\partial}{\partial \xi^3} (A_2^2) \right] \\
& + \frac{\Phi_3^2}{2A_3^4 a^2} \left[ \frac{\Phi_1}{A_1^2} \frac{\partial}{\partial \xi^1} (A_3^2) + \frac{\Phi_2}{A_2^2} \frac{\partial}{\partial \xi^2} (A_3^2) + \frac{\Phi_3}{A_3^2} \frac{\partial}{\partial \xi^3} (A_3^2) \right] = 0,
\end{aligned} \tag{1}$$

where

$$\begin{aligned}
\Phi_i & \equiv \frac{\partial \Phi}{\partial \xi^i}, & \Phi_1 & \equiv \frac{\partial \Phi}{\partial \xi^1}, & \Phi_{ii} & \equiv \frac{\partial^2 \Phi}{\partial (\xi^i)^2}, & \Phi_{11} & \equiv \frac{\partial^2 \Phi}{\partial (\xi^1)^2} \\
\Phi_{ij} & \equiv \frac{\partial^2 \Phi}{\partial \xi^i \partial \xi^j}, & \Phi_{1j} & \equiv \frac{\partial^2 \Phi}{\partial \xi^1 \partial \xi^j}, & i, j & = 2, 3.
\end{aligned}$$

Further, in order to determine the speed of sound  $a$ , we use the Bernoulli energy equation

$$\frac{a^2}{\gamma - 1} + \frac{1}{2} q^2 = \text{constant}.$$

The flow speed is expressed by

$$\begin{aligned}
q^2 & = \frac{\Phi_1^2}{A_1^2} + \frac{\Phi_2^2}{A_2^2} + \frac{\Phi_3^2}{A_3^2} \\
& = u_1^2 + u_2^2 + u_3^2.
\end{aligned}$$

To complete our description of the ellipsoid, on which the boundary condition is satisfied we set

$$\begin{aligned}
\xi^1 & = \xi_0^1 \quad (\text{a constant}) \\
& = \sqrt{\sigma} \ln \bar{\xi}_0^1
\end{aligned}$$

which yields

$$\frac{x^2}{1 + (\xi_0^1)^2} + \frac{y^2}{\sigma + (\xi_0^1)^2} + \frac{z^2}{(\xi_0^1)^2} = 1.$$

On this surface we apply the body-surface boundary-condition

$$\Phi_1 = 0.$$

Since we are concerned, throughout, with bodies without circulation, the boundary condition at infinity is

$$\Phi = \Phi_\infty \quad \text{at} \quad \bar{\xi}^1 = K'(\xi^1 = \infty),$$

here  $\Phi_\infty$  is the undisturbed (freestream) velocity potential.

In this coordinate system, along the hyperbolae  $\xi^2 = \pm K$ ,  $\xi^3 = \pm K'$ , we have  $B_1 = 0$ , implying a vanishing Jacobian of the transformation. It was shown by Duck<sup>6</sup> that along these lines the potential equation reduces simply to

$$\Phi_{22} + \Phi_{33} = 0, \quad (2)$$

and the flow velocity is given by

$$\begin{aligned} q^2 &= \frac{\Phi_1^2}{[\sigma + (\xi^1)^2]^2} + \frac{\Phi_{22}^2 + \Phi_{23}^2}{\sigma(1-\sigma)[\sigma + (\xi^1)^2]} \\ &= \frac{\Phi_1^2}{[\sigma + (\xi^1)^2]^2} + \frac{\Phi_{23}^2 + \Phi_{33}^2}{\sigma(1-\sigma)[\sigma + (\xi^1)^2]}. \end{aligned}$$

A fuller description of the ellipsoidal coordinate system is given in Ref. 6.

### 3. Numerical Techniques

#### 3.1. Finite Differences Equation

We follow the example of Albane<sup>4</sup> and Jameson<sup>5</sup> by rearranging the principal part (that is all terms involving second derivatives) of the potential equation (1) into canonical form, in the following way:

$$(1 - M^2)\Phi_{ss} + \nabla^2 \Phi - \Phi_{ss}$$

where

$$\begin{aligned} \Phi_{ss} &\equiv \frac{1}{q^2} \left[ \frac{u_1^2}{A_1^2} \Phi_{11} + \frac{u_2^2}{A_2^2} \Phi_{22} + \frac{u_3^2}{A_3^2} \Phi_{33} + \frac{2u_1u_2}{A_1A_2} \Phi_{12} + \frac{2u_1u_3}{A_1A_3} \Phi_{13} + \frac{2u_2u_3}{A_2A_3} \Phi_{23} \right], \\ \nabla^2 \Phi &\equiv \frac{1}{A_1^2} \Phi_{11} + \frac{1}{A_2^2} \Phi_{22} + \frac{1}{A_3^2} \Phi_{33}, \end{aligned}$$

and  $M = q/a$  is the local Mach number.

The first order derivatives of (1) remain unchanged.

For the purposes of computation, the total potential  $\Phi$  is now split up in the form

$$\Phi = \Phi_\infty + \phi,$$

where  $\Phi_\infty$  denotes the freestream (undisturbed) potential, and is a known quantity, with a singularity at infinity—we solve only for  $\phi$ , the perturbation (unknown) potential.

The partial differential equation is now ready to be differenced.

Assuming  $l_m + 1$ ,  $m_m + 1$ ,  $n_m + 1$  points in the  $\xi^1$ ,  $\xi^2$  and  $\xi^3$  directions respectively, then the cell dimensions in the differenced system (for the general case), are given by

$$\Delta \xi^1 = (K' - \xi_0^1)/l_m,$$

$$\Delta \xi^2 = 4K/m_m$$

and

$$\Delta \xi^3 = 2K'/n_m.$$

The coefficients of  $K$  and  $K'$  in the above expressions for  $\Delta \xi^2$  and  $\Delta \xi^3$  may be reduced if any symmetry is present in the problem.

All first derivatives of  $\phi$  are differenced centrally throughout the entire flow field, for example

$$(\phi_3)_{l,m,n} = \frac{\phi_{l,m,n+1} - \phi_{l,m,n-1}}{2\Delta\xi^3} + O((\Delta\xi^3)^2)$$

(where  $l, m, n$  identify the point in the field).

Second derivatives of  $\phi$  contained within  $\nabla^2\Phi - \Phi_{ss}$  are also centrally differenced, for example

$$(\phi_{33})_{l,m,n} = \frac{\phi_{l,m,n+1} - 2\phi_{l,m,n} + \phi_{l,m,n-1}}{(\Delta\xi^3)^2} + O((\Delta\xi^3)^2)$$

and

$$(\phi_{23})_{l,m,n} = \frac{\phi_{l,m+1,n+1} - \phi_{l,m-1,n+1} - \phi_{l,m+1,n-1} + \phi_{l,m-1,n-1}}{4\Delta\xi^2\Delta\xi^3} + O((\Delta\xi^2)^2(\Delta\xi^3)^2).$$

For elliptic (subcritical) points the second derivatives of  $\phi$  contained within  $(1-M^2)\Phi_{ss}$  are differenced centrally, as above. However for hyperbolic (supercritical) points, the differencing is non-central, for example

$$(\phi_{33})_{l,m,n} = \frac{\phi_{l,m,n} - 2\phi_{l,m,n+1} + \phi_{l,m,n+2}}{(\Delta\xi^3)^2} + O(\Delta\xi^3),$$

where the positive (negative) sign is taken for  $\Phi_3$  negative (positive).

Similarly

$$(\phi_{23})_{l,m,n} = \text{sign}(\Phi_2\Phi_3) \frac{\phi_{l,m,n} - \phi_{l,m+1,n} - \phi_{l,m,n+1} + \phi_{l,m+1,n+1}}{\Delta\xi^2\Delta\xi^3} + O(\Delta\xi^2 + \Delta\xi^3)$$

where the signs are chosen depending on the signs of  $\Phi_2$  and  $\Phi_3$ .

Along the singular lines, we use equation (2), which is elliptic, for both subcritical and supercritical points, central differencing always being applied to this equation. Points on either side of these singular points, in the  $\xi^2$  and  $\xi^3$  directions are in fact equivalent, due to the periodicity of the working space (see Fig. 1).

Symmetry arguments may be invoked (if present) in order to reduce both computer time and store requirements. For flows with freestream velocities aligned along one of the axes of the ellipsoid, two quadrants are required for supercritical calculations (the fore and aft anti-symmetry of subcritical cases is no longer present).

Referring to Fig. 1, if  $\Phi_\infty = x$ , any adjacent combination of quadrants A and B (or C and D) may be used. Symmetry may then be invoked along the perimeter of each plane  $\xi^1 = \text{constant}$ , because of the up and down, and side to side symmetry present. If  $\Phi_\infty = y$ , any adjacent combination of quadrants A and C (or B and D) may be used. In addition to symmetry considerations, the periodicity of the working space must be taken into account. As an example, consider the plane  $\xi^1 = \text{constant}$  over the region

$$0 \leq \xi^2 \leq K$$

$$0 \leq \xi^3 \leq 2K'$$

as shown hatched in Fig. 1. Symmetry may be invoked along OORSO, but not along OTO. But because of periodicity, a point such as V, described in ellipsoidal coordinates by  $(\xi^1, K + \Delta\xi^2, \xi^3)$  maps to the same point in cartesian (physical) space as the point  $(\xi^1, K - \Delta\xi^2, 2K' - \xi^3)$  in the working space. Similar arguments apply to other combinations of B and D (or A and C).

For yawed cases, more quadrants must be brought into the calculations, with arguments similar to those given above invoked in order to 'close' the working space.

Finally we apply the body surface boundary condition by means of reflection.

If  $\xi_0^1 \leq \xi^1 \leq K'$  as  $1 \leq l \leq l_m + 1$  then

$$\phi_{0,m,n} = \phi_{2,m,n} + 2\Delta\xi^1(\Phi_{\infty 1})_{\text{body surface}}.$$

This then gives values of  $\phi$  for the set of points situated just inside the body that are required in the difference equation.

### 3.2. Solution of Difference Equation

The difference equation may now be expressed in a form suitable for line relaxation. For solution along lines  $\xi^2, \xi^3 = \text{constant}$  (spokes), the difference equation may be expressed in standard tridiagonal form

$$b_l \phi_{l+1,m,n} + c_l \phi_{l,m,n} + d_l \phi_{l-1,m,n} = a_l \quad \text{for } 1 \leq l \leq l_m (\phi_{l_m+1,m,n} = 0)$$

where  $b_{l_m} = 0$  and  $d_1 = 0$ .

As many terms as possible are placed on the left-hand side of the above equation, the remainder, including all the second order derivatives of the freestream contribution to the potential and also most of the contributions in the difference equation from other mesh points, being placed on the right-hand side.

The resulting matrix equation for  $\phi$  may be solved using the well known Choleski method (see for example Varga<sup>7</sup>).

Having solved for  $\phi$  in this way, we apply relaxation to update the old value of  $\phi$

$$\phi_{l,m,n}^{(N)} = \omega \phi_{l,m,n} + (1 - \omega) \phi_{l,m,n}^{(N-1)},$$

$\phi_{l,m,n}$  being obtained from the block inversion described above, and superscript  $(N)$  denotes the value obtained (after relaxation) from the  $N$ th iteration.

The relaxation parameter,  $\omega$ , was usually set at 1.8 in elliptic regions, and 0.96 in hyperbolic regions at the start of the computation, and was reduced if instability occurred. Frequently the computation would undergo a period of instability, during which the relaxation parameters were reduced. The numerical process would then become stable again, and the relaxation parameters could then be increased without further instability.

The direction of 'sweeping' of the lines along which the solution was obtained was varied, including following the flow and directly opposed to the flow, with identical results.

The region close to the shock was usually very slow to convergence during the iteration process. Often the solution in this region would still be changing markedly, whilst in the rest of the flow field, the solution had settled down. For this reason convergence was usually assumed when the maximum change in potential, anywhere within the field was less than  $1 \times 10^{-6}$  per iteration. This implies convergence of Mach number of approximately  $5 \times 10^{-5}$  per iteration.

The shock region also appears the most sensitive to changes in mesh size as shown in the example in Table 1 which refers to the case illustrated in Figs. 2 to 6—presumably this is a result of the large gradients of the potential around the shock (situated near  $y = 0.45$ ). Table 1 indicates that accuracy requires a particularly large number of points in the  $\xi^2$  direction which approximately corresponds to the direction normal to the shock. Most calculations for the unyawed cases were performed using a  $21 \times 21 \times 41$  mesh in the  $\xi^1, \xi^2$  and  $\xi^3$  directions respectively, whilst those for yawed cases were made on a  $21 \times 41 \times 41$  mesh. With these two grids, the Mach numbers appear in general accurate to within about  $\frac{1}{2}$  per cent.

To reduce computation time, the calculation was started on a coarse grid and continued on a medium grid (of half the original cell dimensions), before being transferred to a fine grid (of a quarter the original cell dimensions). Supercritical examples take about 10 times the number of iterations, and about 20 times the computer time of comparable subcritical examples. A typical unyawed, supercritical case takes about 19 minutes on a CDC 7600 computer, with 100 iterations on the two coarse grids, and 600 on the fine grid. Yawed supercritical cases take about double the number of iterations and four times the computer time of comparable unyawed examples.

## 4. Results

By means of a number of linear interpolation routines, the converged solutions were used to produce various Mach number distributions in cartesian  $(x, y, z)$  space, both on the body, and also out into the flow field. Several of these distributions are presented in Figs. 2 to 33 (as shown listed in Table 2). It should be realised that, because of the nature of the interpolation, the distributions away from the body, in particular, should be treated with a certain amount of caution, because of the lower density of points as infinity is approached in the physical field.

Figs. 2 to 11 show distributions of Mach number around two different bodies, with flows aligned along the second major axis ( $\Phi_x = y$ ). The first body (hereafter referred to as body I) has a ratio of axes

1:0.7089:0.0709 in the  $x:y:z$  directions respectively, whilst the second body (referred to as body II) has a corresponding ratio of axes of 1:0.2010:0.0200. Figs. 12 to 16 show the flow around body I with a free-stream flow aligned along the major axis ( $\Phi_\infty = x$ ). For all these examples, it appears that the Mach number across the maximum 'span' of the body is approximately constant, although the examples of higher aspect ratio exhibit a slight increase in Mach number in the region of the tips (see Figs. 4, 9, 14). The exact incompressible solution predicts constant flow speed across the maximum 'span' of the ellipsoid. For the high-aspect-ratio body (Fig. 8) there appears to be a tendency for the position of the maximum Mach number to move away from the plane of symmetry and consequently there may be an increase in shock strength as the 'tips' are approached. For the low-aspect-ratio body (Fig. 13) the opposite occurs and away from the plane of symmetry the shock wave appears to disperse progressively into a distributed compression. Figs. 6, 11, 16 show the flow field in depth in the plane of symmetry and emphasize the increasing departure of the flow from fore-and-aft symmetry as the freestream Mach number increases. Further the shocks appear to meet the body surface approximately perpendicularly. Figs. 3, 13 indicate, in the strongest regions of the shock, after an initial rapid compression, a very weak expansion, followed by a second compression. (This effect is most marked in the example of Fig. 13.) For reference, the positions of the grid points along the centreline are shown in these figures. All other results were obtained by interpolation. Along the centre line the shock is smeared over two or three mesh points. It is expected that, because of the more favourable distribution of 'calculating' points for the  $\Phi_\infty = x$  example (the shock occurs in the region of one of the singular points on the body, a region in which there is a natural 'clustering' of mesh points in the  $x$ -direction) the shock definition is rather better than in the other examples.

Downstream of the shock, the Mach number distributions appear to almost 'regain' the symmetry of subcritical flows, the Mach number at a position behind and away from the shock matching closely with that at the corresponding position upstream of the shock. Details of subcritical flows past unyawed ellipsoids are given in Ref. 6.

Distribution of Mach numbers for flows around body I, with the freestream flow inclined at 45 degrees to the  $x$  and  $y$  axes ( $\Phi_\infty = (x + y)/\sqrt{2}$ ) are shown in Figs. 17 to 26. Figs. 17 to 19 are for a subcritical example ( $M_\infty = 0.8$ ), for comparison with a supercritical case ( $M_\infty = 0.945$ ), details of which are given in Figs. 20 to 26.

The structure of the shock for this supercritical example is similar to that of the unyawed examples discussed previously.

The acceleration following the rapid compression this time results in a second (just) supersonic zone, before the second compression (see Fig. 21).

The position of the stagnation points, in comparison with the subcritical case appear little changed, in spite of the appearance of a shock. Again, well away from the shock, the flow appears to regain the symmetry of Mach number distribution present in the subcritical example (Figs. 17 and 20).

Figs. 27 to 33 refer to the flow around body II with freestream flow inclined at 45 degrees to the  $x$  and  $y$  axes, with  $M_\infty = 0.97$ .

The main characteristic of these figures is the absence of any noticeable shock, the flow appearing still to have the symmetry associated with totally subcritical flows.

Finally, it should be stressed that, since the Rankine-Hugoniot relations have not been satisfied across any shock (only continuity of potential is satisfied) then the actual structure and position of any shocks arising from these calculations should be treated with caution.

## 5. Conclusions

It has been shown that numerical solutions may be obtained for the supercritical flow around ellipsoids without circulation and under steady, inviscid conditions.

Although the Rankine-Hugoniot equations have not been applied, the full equations of motion (in ellipsoidal coordinate form) have been used and the boundary condition on the surface of the ellipsoid has been applied as exactly as the differencing schemes allow. Using a transformation of one of the coordinates, the entire flow field has been brought into a finite computation space. Shocks appear in the converged solutions, generally smeared over two or three grid points.

The numerical scheme, using the proportion of central and non-central differencing as suggested by Albane<sup>4</sup> and Jameson<sup>5</sup> has generally been reliable with only intermittent outbreaks of instability. Computation times, however, are still appreciably longer than their subcritical counterparts, primarily because of the slow convergence at points in the neighbourhood of the shock.

**Acknowledgments**

The author wishes to thank Professor K. W. Mangler for many valuable discussions and comments in connection with this problem. The financial assistance of the SRC is gratefully acknowledged. The computations were carried out at the Computing Centre, University of Southampton, using the link to the U.L.C.C. C.D.C. 7600.

# LIST OF SYMBOLS

$a$	Speed of sound
$a_i, b_i, c_i, d_i$	Coefficients in matrix equation
$A_i$	Curvilinear metrics
$B_i$	Magnitudes relating to the $A_i$
$K(K')$	(Complementary) complete elliptic integrals of the first kind
$l_{m+1}, m_{m+1}, n_{m+1}$	Number of points in $\xi^1, \xi^2, \xi^3$ directions
$M$	Mach number
$q$	Flow speed
$u_i$	$\Phi_i/A_i$ velocity component in $\xi^i$ direction
$x, y, z$	Cartesian coordinates
$\gamma$	Ratio of specific heats
$\xi^1, \xi^2, \xi^3$	Ellipsoidal coordinates
$\bar{\xi}^1$	Transformed $\xi^1$ coordinate
$\sigma$	Body description parameter
$\phi$	Perturbation potential
$\Phi$	Total potential $\Phi_\infty + \phi$
$\Phi_\infty$	Freestream (undisturbed) potential
$\Phi_i$	$\partial\Phi/\partial\xi^i$ ( $i = 2, 3$ ); $\partial\Phi/\partial\bar{\xi}^1$ ( $i = 1$ )
$\Phi_{ij}$	$\partial^2\Phi/\partial\xi^i \partial\xi^j$ ( $i = 2, 3$ ); $\partial^2\Phi/\partial\bar{\xi}^1 \partial\xi^i$ ( $i = 1$ )
$\Phi_{ss}$	Second derivative in streamwise direction
<i>Subscripts</i>	
$i, j, k$	Indices running from 1 to 3
$l, m, n$	Indices identifying points in field
$0$	Body surface conditions
$\infty$	Freestream conditions
<i>Superscripts</i>	
$i, j, k$	Indices running from 1 to 3
$N$	Value obtained from $N$ th iteration

## REFERENCES

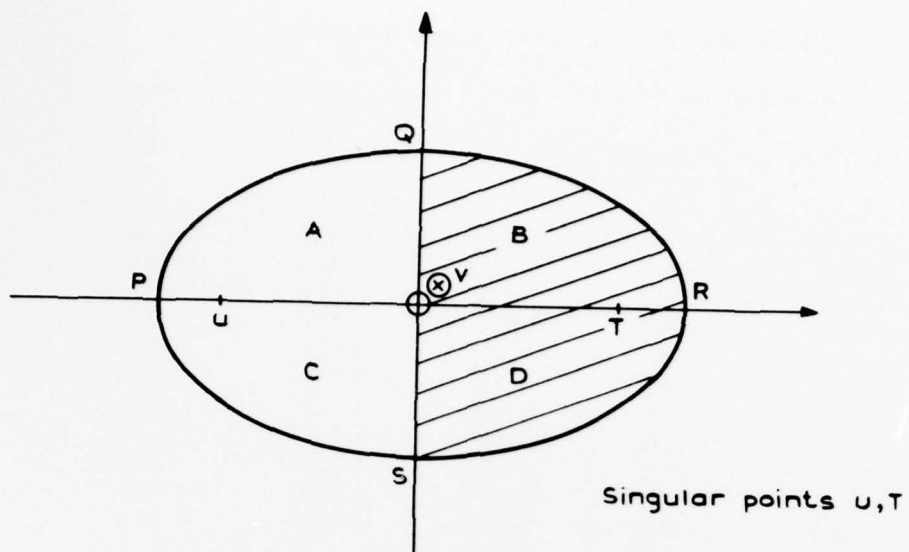
- | <i>No.</i> | <i>Author(s)</i>                        | <i>Title, etc.</i>   |
|------------|---|--|
| 1          | R. Magnus and H. Yoshihara . . . . .    | Inviscid transonic flow over airfoils.<br>A.I.A.A. Journal, Vol. 8, pp. 2157-2162, 1970.   |
| 2          | E. M. Murman and J. D. Cole . . . . .   | Calculation of plane steady transonic flows.<br>A.I.A.A. Journal, Vol. 9, pp. 114-121, 1971.   |
| 3          | P. R. Garabedian and D. G. Korn . . . . | Analysis of transonic airfoils.<br>Communs. pure appl. Math., Vol. 24, pp. 841-851, 1971.  |
| 4          | C. M. Albone . . . . .                  | A finite-difference scheme for computing supercritical flows in<br>arbitrary coordinate systems.<br>A.R.C. C.P. No. 1313, 1974.                        |
| 5          | A. Jameson . . . . .                    | Iterative solution of transonic flows over airfoils and wings,<br>including flows at Mach 1.<br>Communs. pure appl. Math., Vol. 27, pp. 283-309, 1974. |
| 6          | P. W. Duck . . . . .                    | The numerical calculation of subcritical steady potential flow<br>around an unyawed ellipsoid.<br>A.R.C. R. & M. No. 3795, 1977.                       |
| 7          | R. S. Varga . . . . .                   | Matrix iterative analysis.<br>Prentice-Hall, N.J., 1962..  |

TABLE 1  
Variation of Mach Number on Body Surface with Mesh Size Along  
 $x = 0, \Phi_{\infty} = y, M_{\infty} = 0.92, \sigma = 0.5$

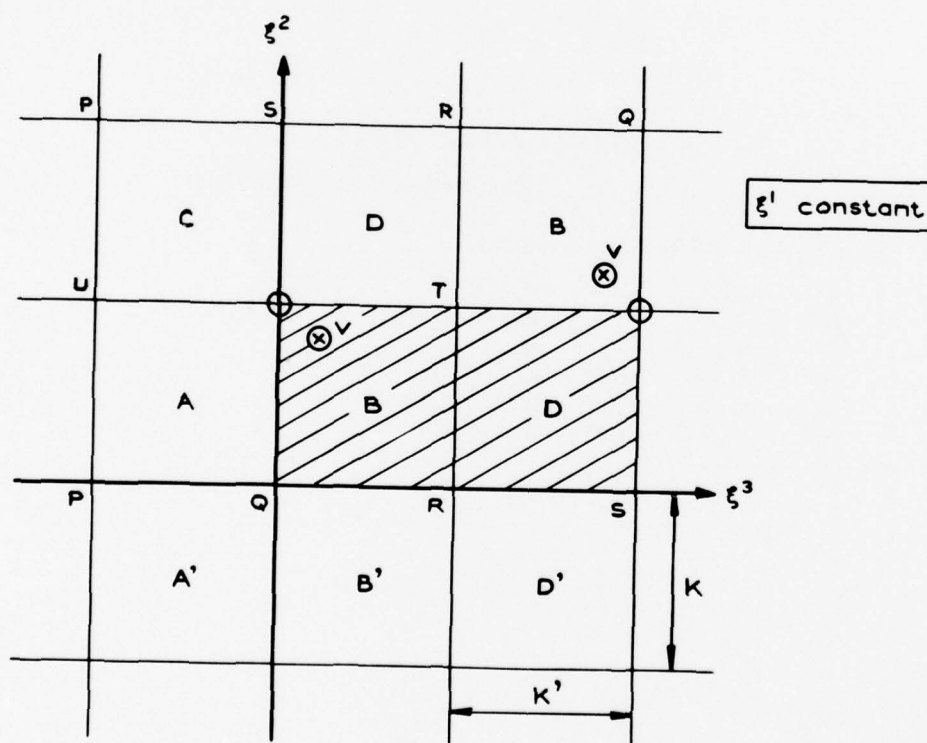
mesh y	$21 \times 21 \times 41$	$15 \times 15 \times 29$	$15 \times 21 \times 41$	$21 \times 15 \times 41$	$21 \times 21 \times 29$
-0.7107	0.0000	0.0000	0.0000	0.0000	0.0000
-0.5685	0.9925	0.9916	0.9913	0.9929	0.9925
-0.4264	1.0439	1.0422	1.0427	1.0435	1.0439
-0.2843	1.0758	1.0740	1.0747	1.0752	1.0757
-0.1421	1.1028	1.1011	1.1017	1.1024	1.1026
0	1.1299	1.1285	1.1288	1.1299	1.1296
+0.1421	1.1604	1.1599	1.1593	1.1613	1.1601
+0.2843	1.1991	1.1998	1.1980	1.2014	1.1990
+0.4264	1.1388	1.1212	1.1326	1.1264	1.1381
+0.5685	0.9881	0.9867	0.9872	0.9873	0.9883
+0.7107	0.0000	0.0000	0.0000	0.0000	0.0000

TABLE 2  
Details of Calculations Presented

Body I: $\sigma = 0.5 \quad \bar{\xi}_0^1 = 0.1$			
Ratio of axes: 1:0.7089:0.0707			
Body II: $\sigma = 0.04 \quad \bar{\xi}_0^1 = 0.1$			
Ratio of axes: 1:0.2010:0.0200			
$\gamma$			
Figures	Body	Freestream conditions	
2-6	I	$\Phi_{\infty} = y$	$M_{\infty} = 0.92$
7-11	II	$\Phi_{\infty} = y$	$M_{\infty} = 0.88$
12-16	I	$\Phi_{\infty} = x$	$M_{\infty} = 0.97$
17-19	I	$\Phi_{\infty} = (x+y)/\sqrt{2}$	$M_{\infty} = 0.80$
20-26	I	$\Phi_{\infty} = (x+y)/\sqrt{2}$	$M_{\infty} = 0.945$
27-33	II	$\Phi_{\infty} = (x+y)/\sqrt{2}$	$M_{\infty} = 0.97$



a Physical plane (planform)



b Working plane

FIG. 1a & b. Layout of physical plane and of working plane.

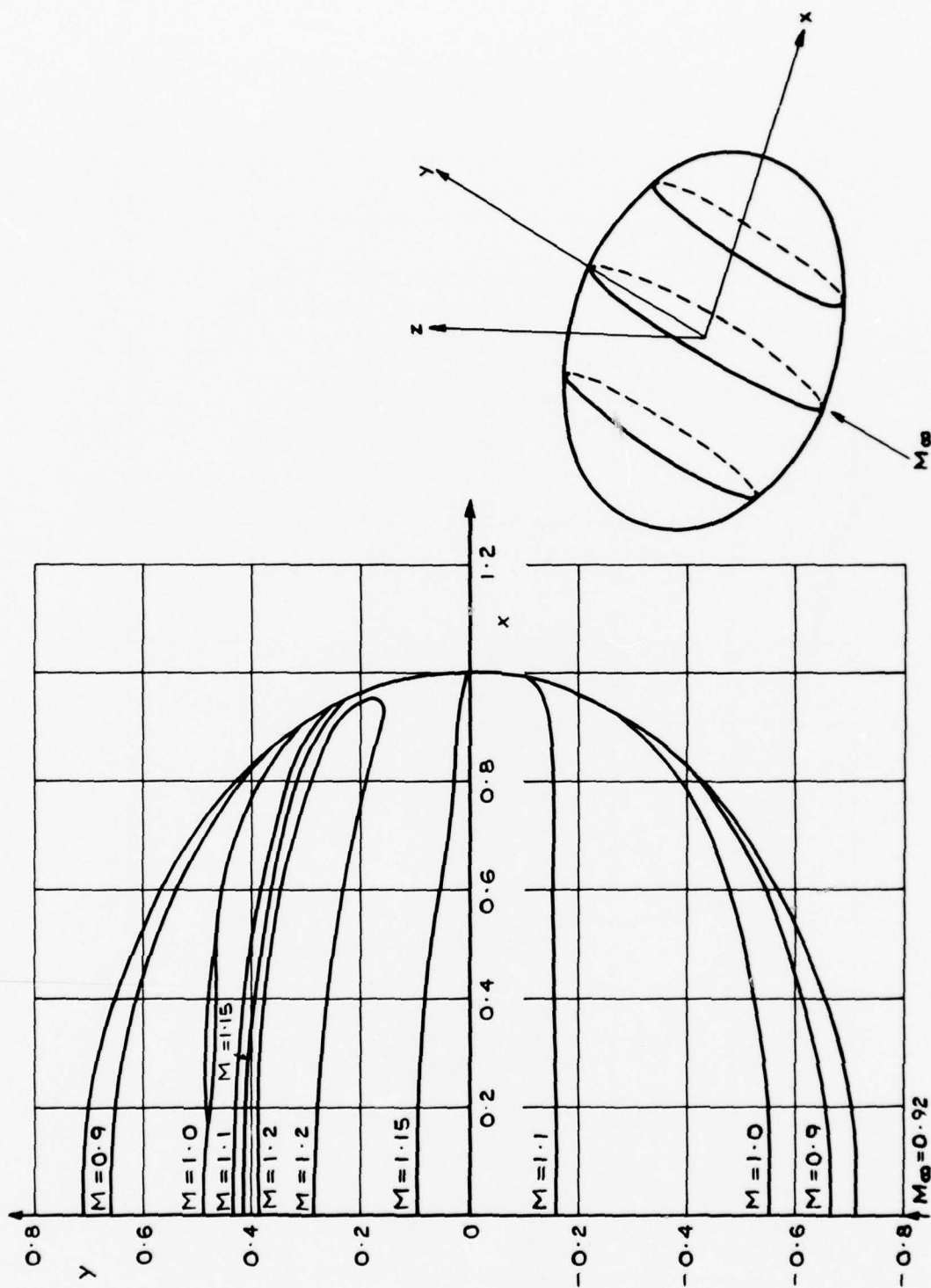


Fig. 2. Lines of constant Mach number on body surface  $M_\infty = 0.92 \Phi_x = y$  Body I.

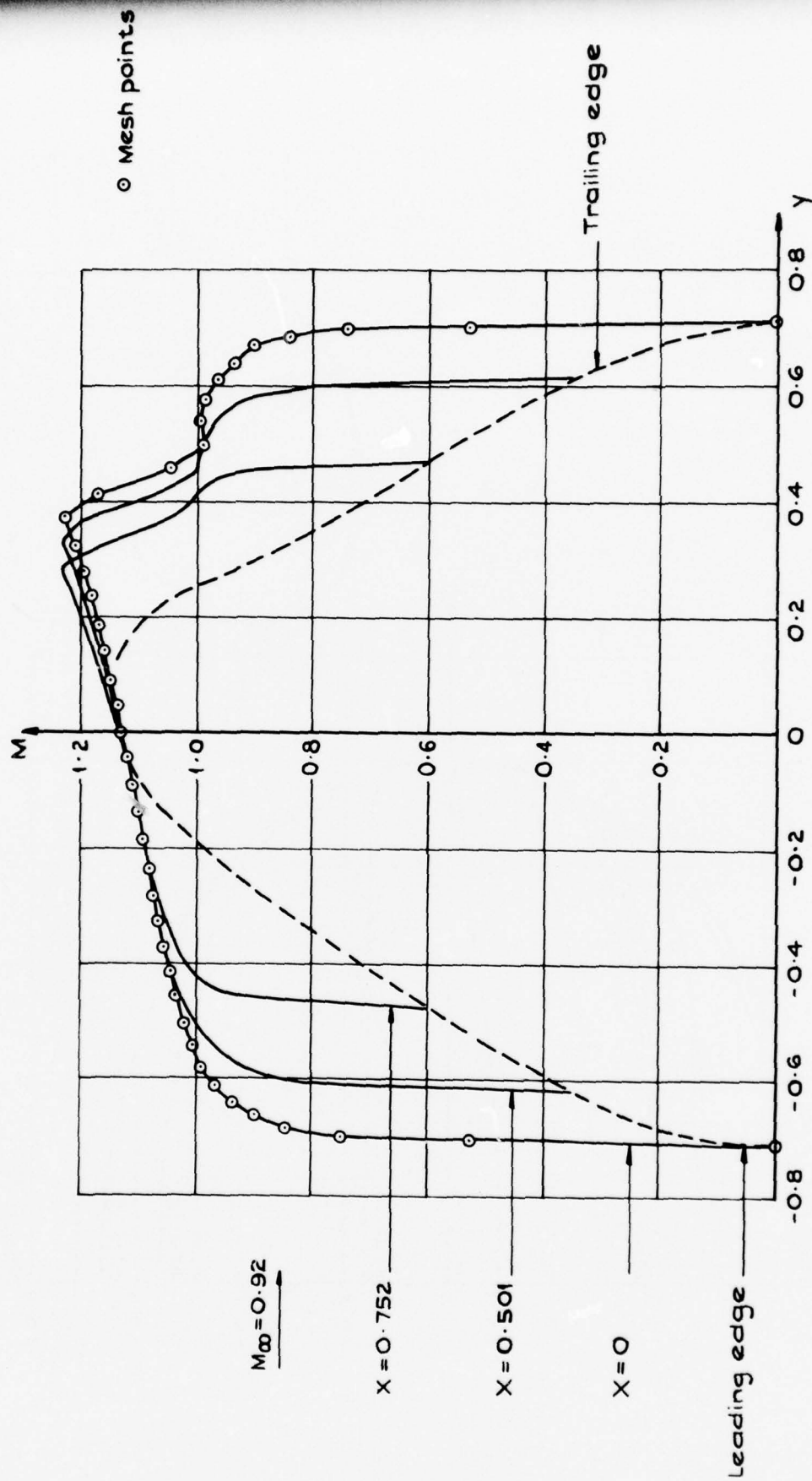


FIG. 3. Mach number distributions along lines  $x = \text{constant}$  on body surface  $M_\infty = 0.92$   $\Phi_\infty = y$  Body I.

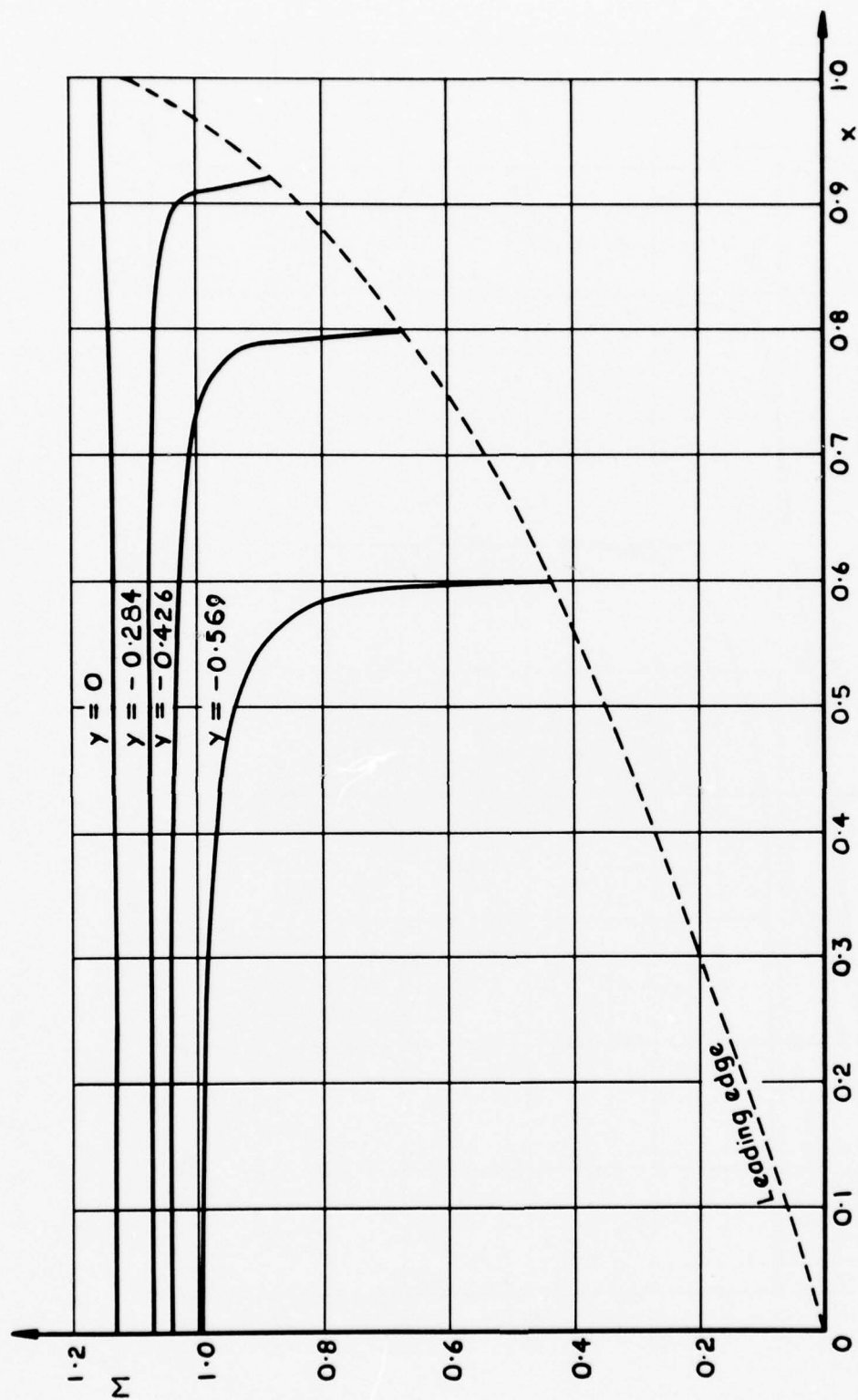


FIG. 4. Mach number distributions along lines  $y = \text{constant}$  on body surface ( $y \leq 0$ )  $M_\infty = 0.92$   $\Phi_x = y$  Body I.

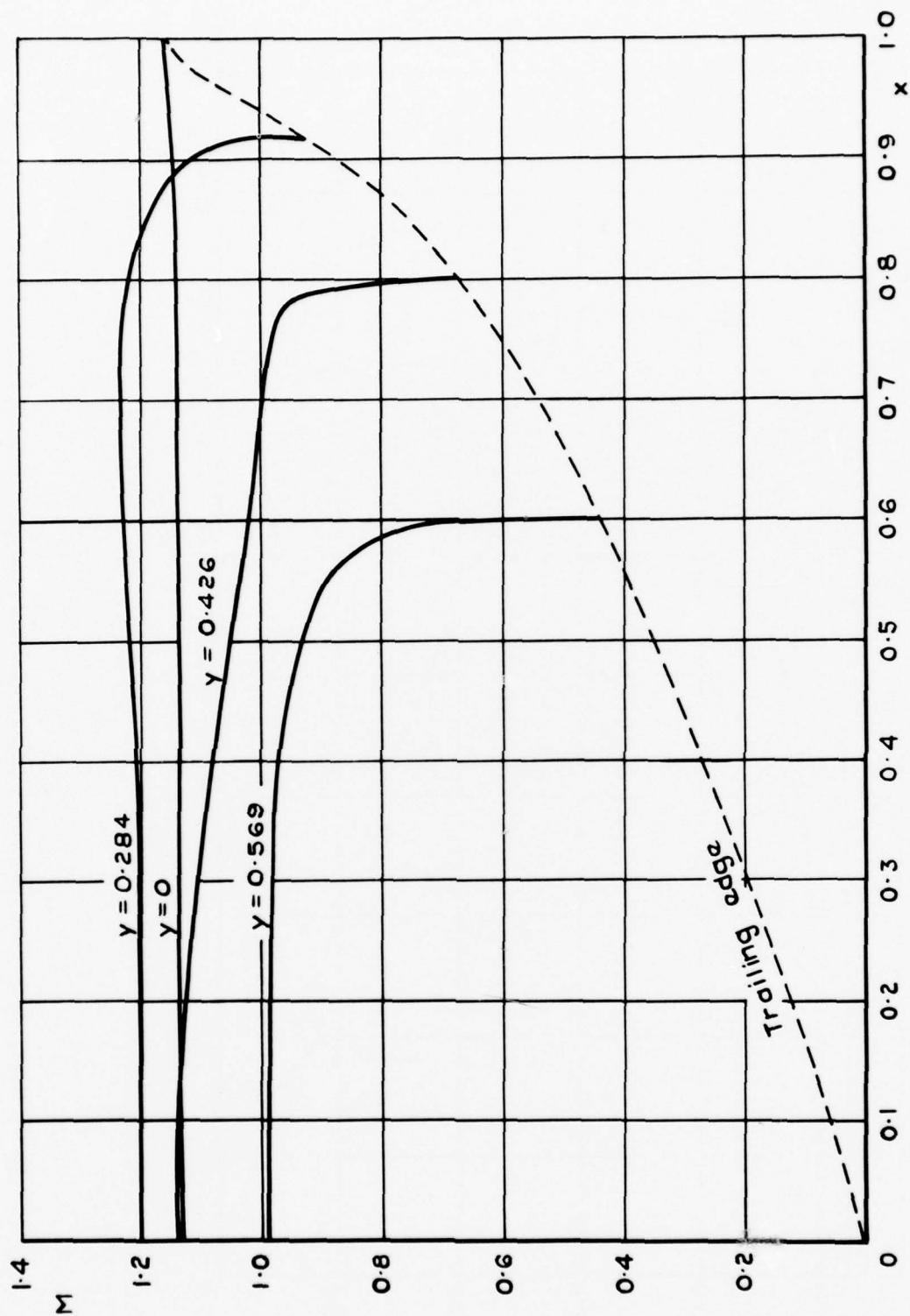
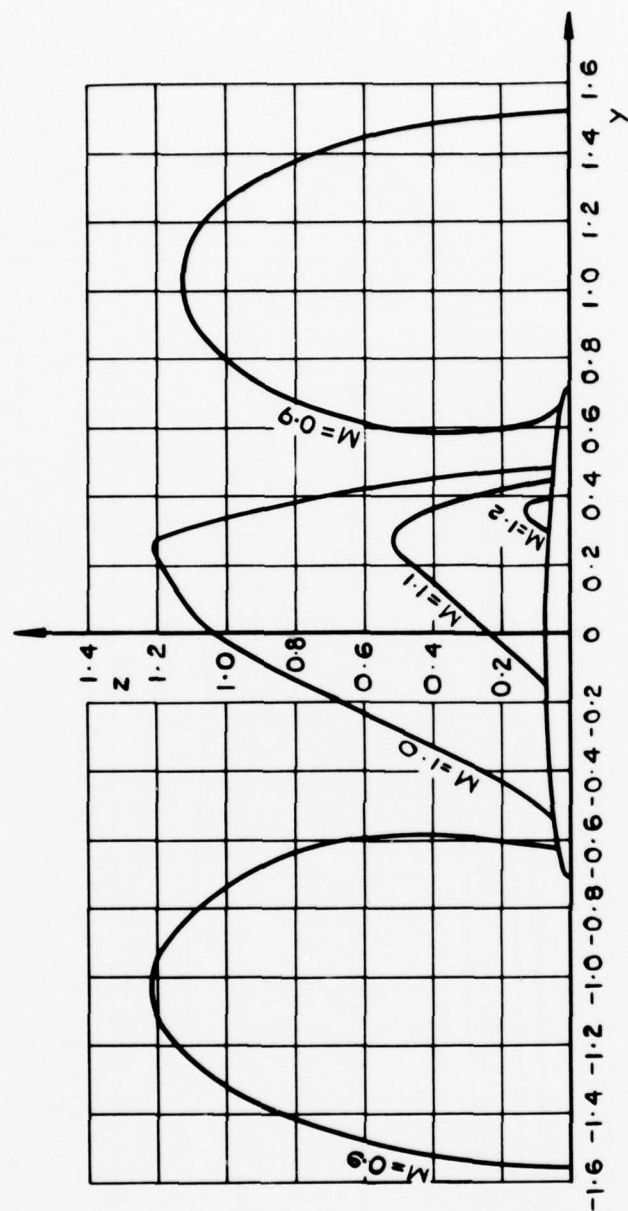


FIG. 5. Mach number distributions along lines  $y = \text{constant}$  on body surface ( $y \geq 0$ )  $M_\infty = 0.92$   $\Phi_\infty = y$  Body I.



$M_{\infty} = 0.92$

FIG. 6. Lines of constant Mach number in the plane  $x = 0$   $M_{\infty} = 0.92$   $\Phi_{\infty} = y$  Body I.

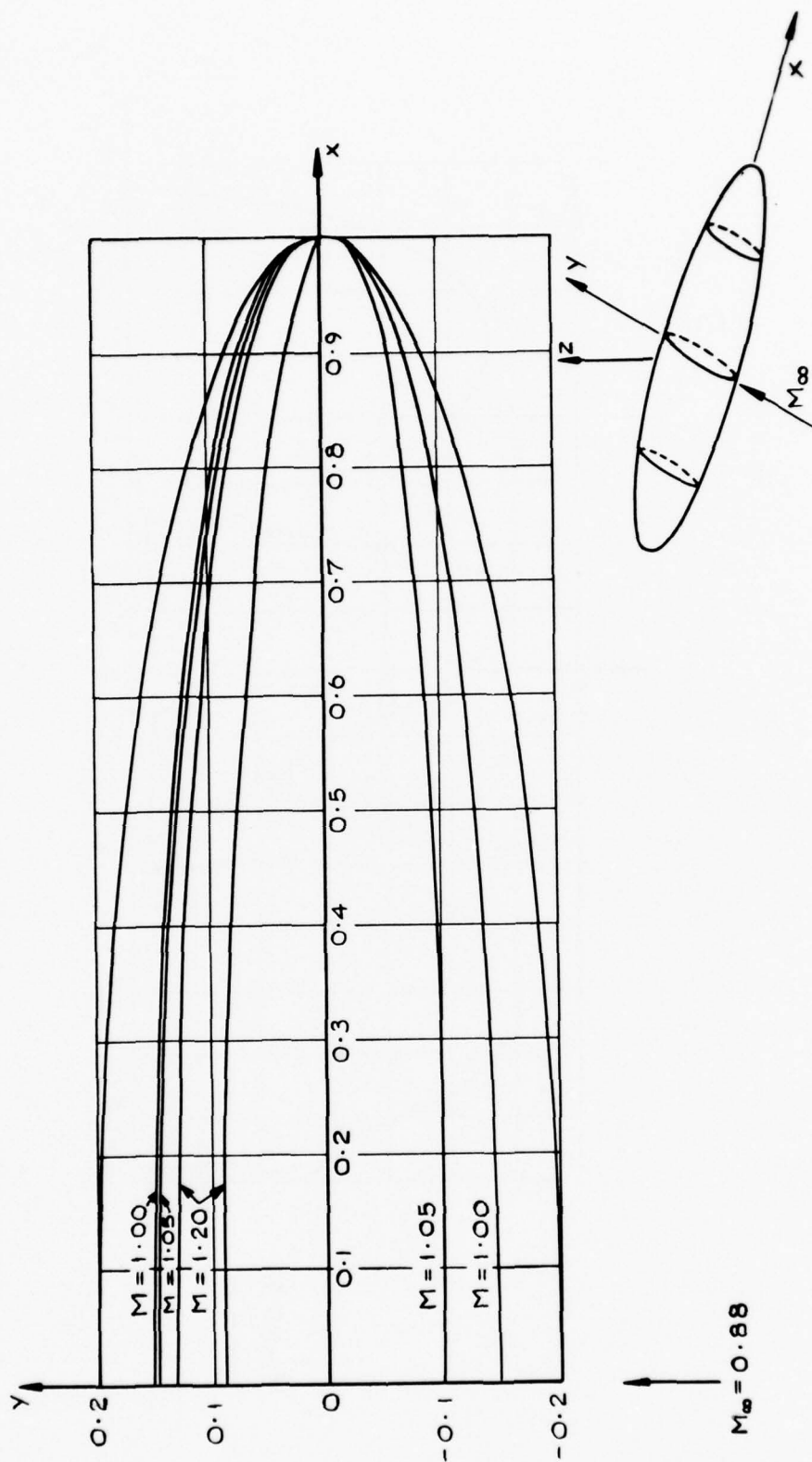


FIG. 7. Lines of constant Mach number on body surface  $M_x = 0.88 \phi_x = y$  Body II.

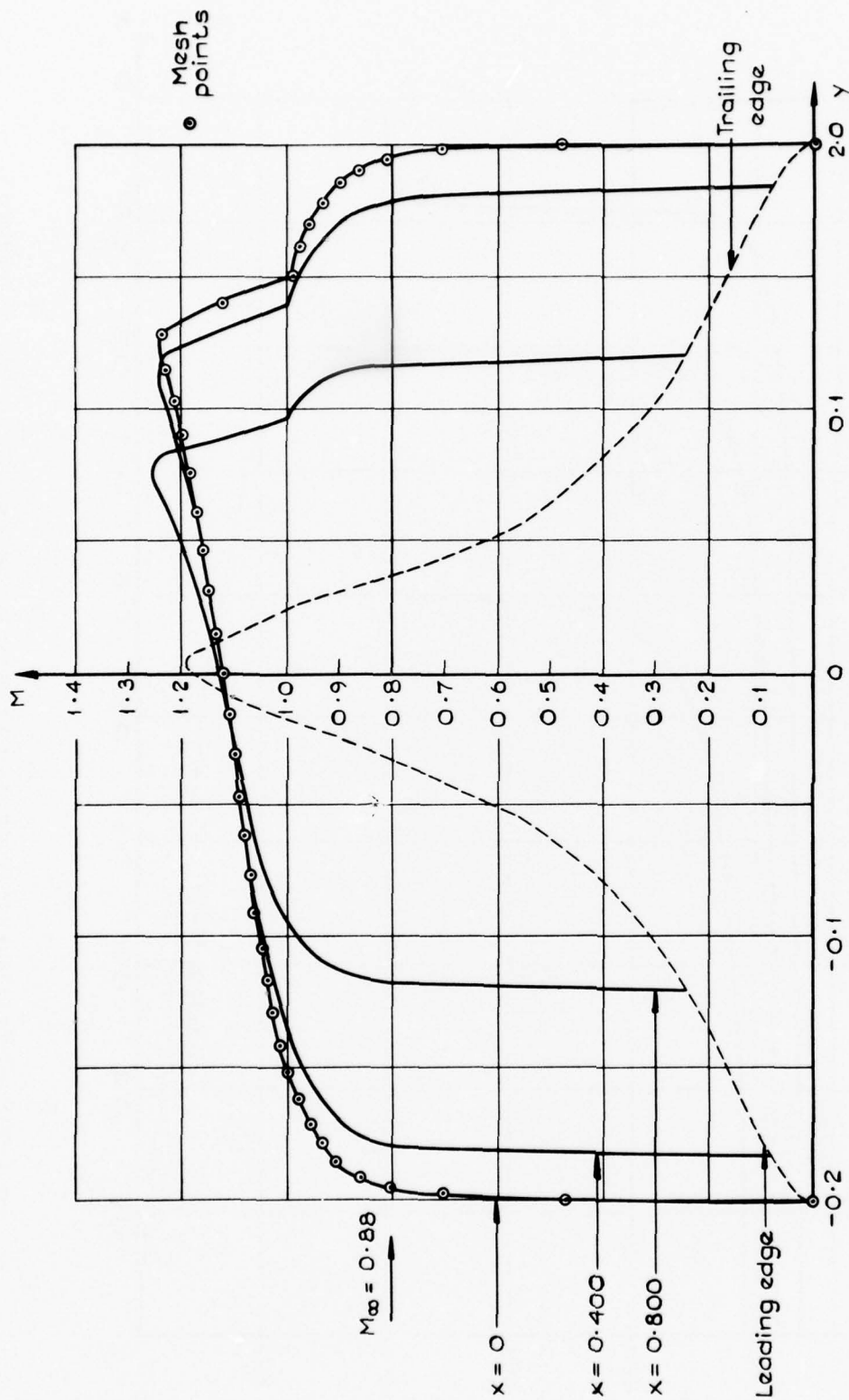


FIG. 8. Mach number distributions along lines  $x = \text{constant}$  on body surface  $M_\infty = 0.88$   $\Phi_x = y$  Body II.



FIG. 9. Mach number distributions along lines  $y = \text{constant}$  on body surface ( $y \leq 0$ )  $M_\infty = 0.88$   $\Phi_\infty = y$  Body II.

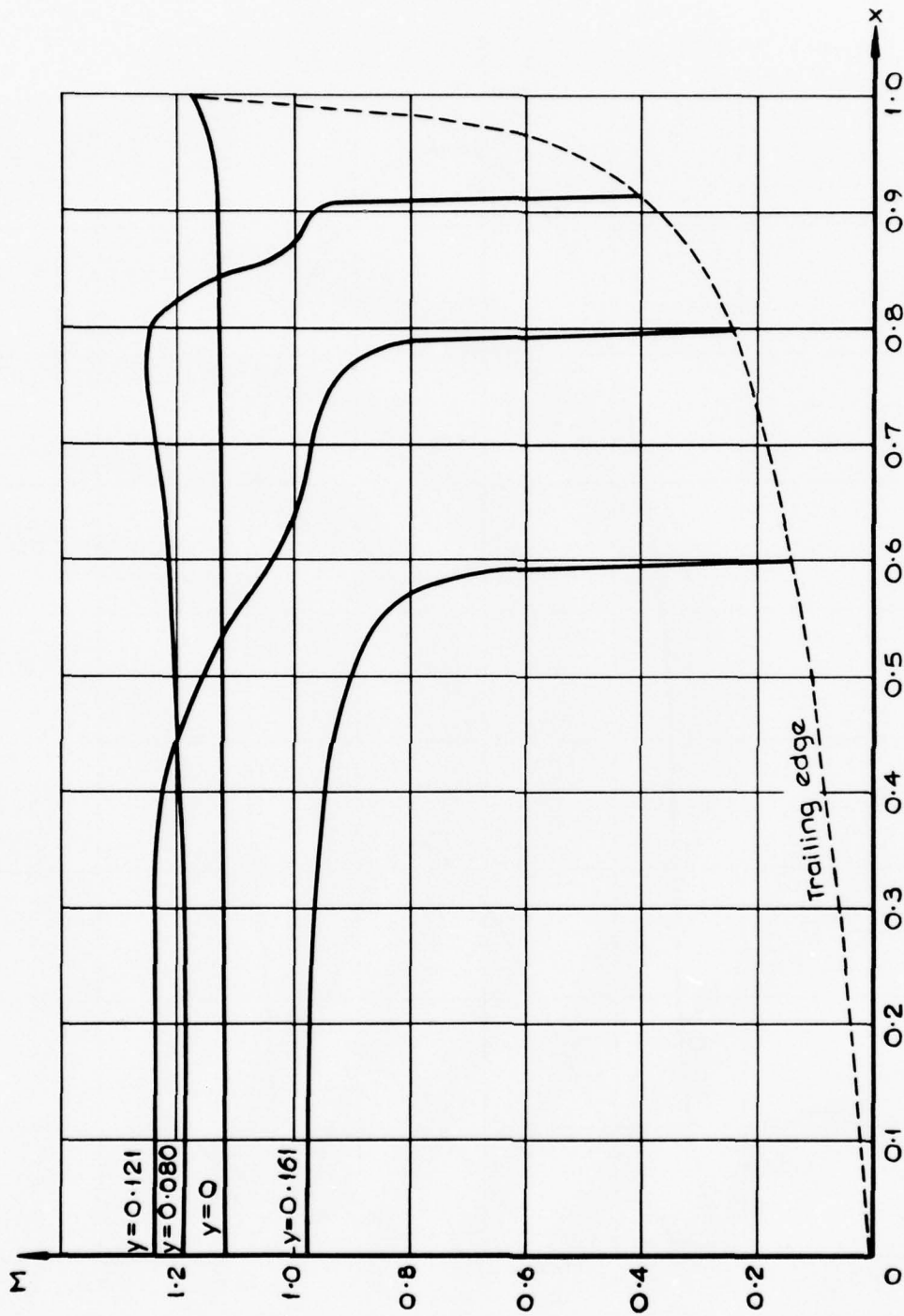


FIG. 10. Mach number distributions along lines  $y = \text{constant}$  on body surface ( $y \geq 0$ )  $M_\infty = 0.88$   $\phi_x = y$  Body II.

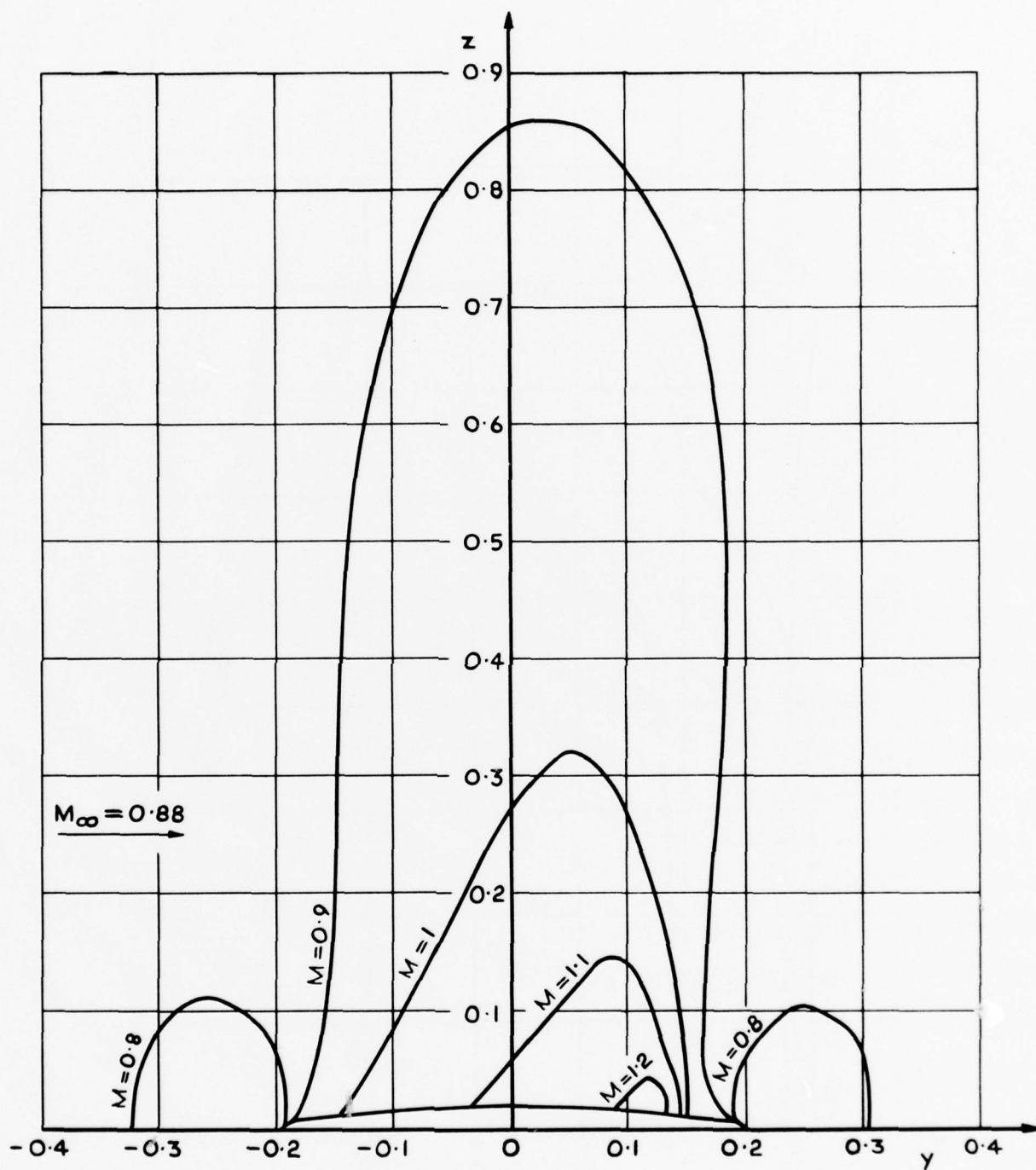


FIG. 11. Lines of constant Mach number in the plane  $x = 0$   $M_\infty = 0.88$   $\Phi_\infty = y$  Body II.

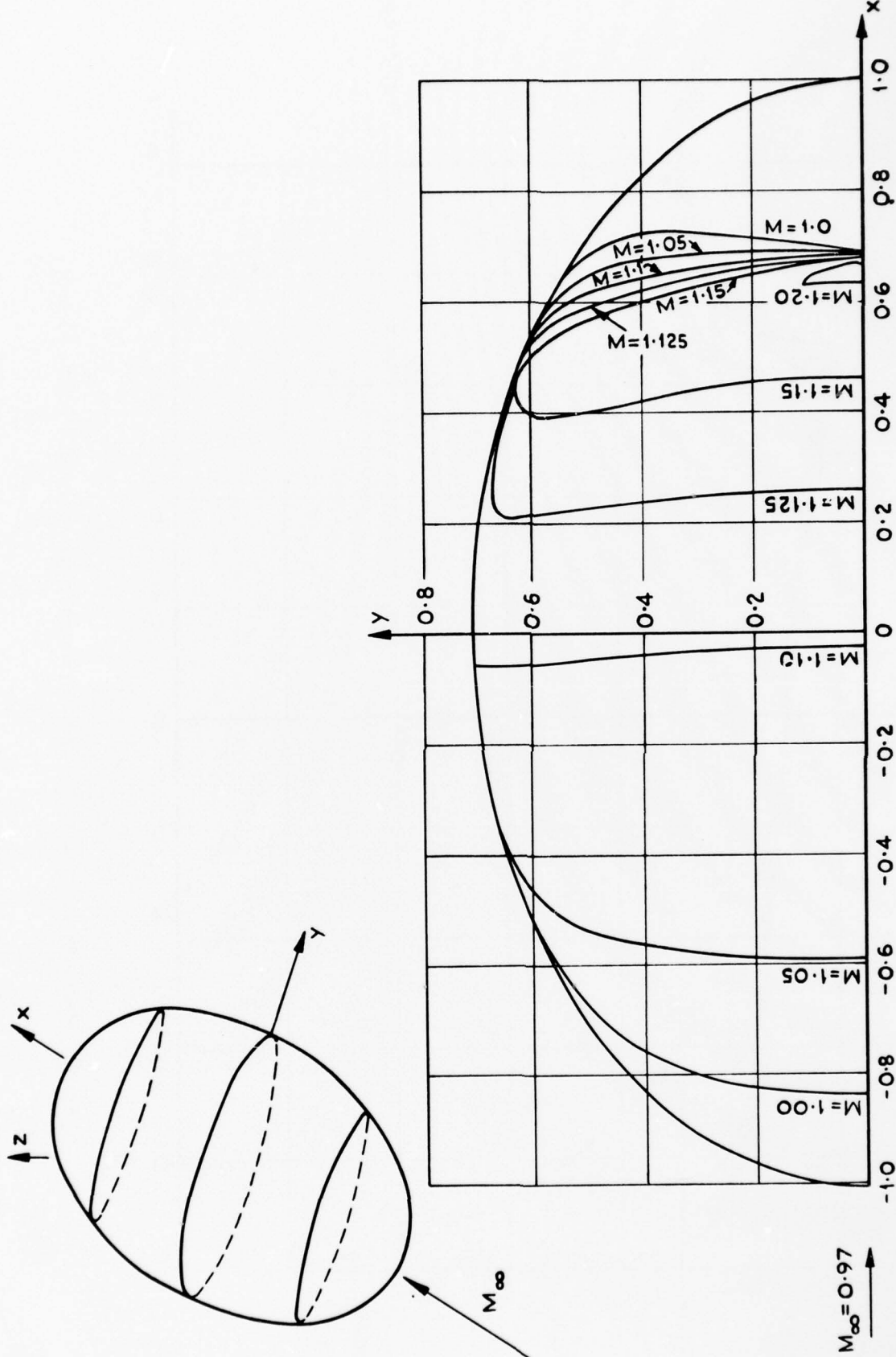


FIG. 12. Lines of constant Mach number on body surface  $M_\infty = 0.97 \Phi_x = x$  Body I.

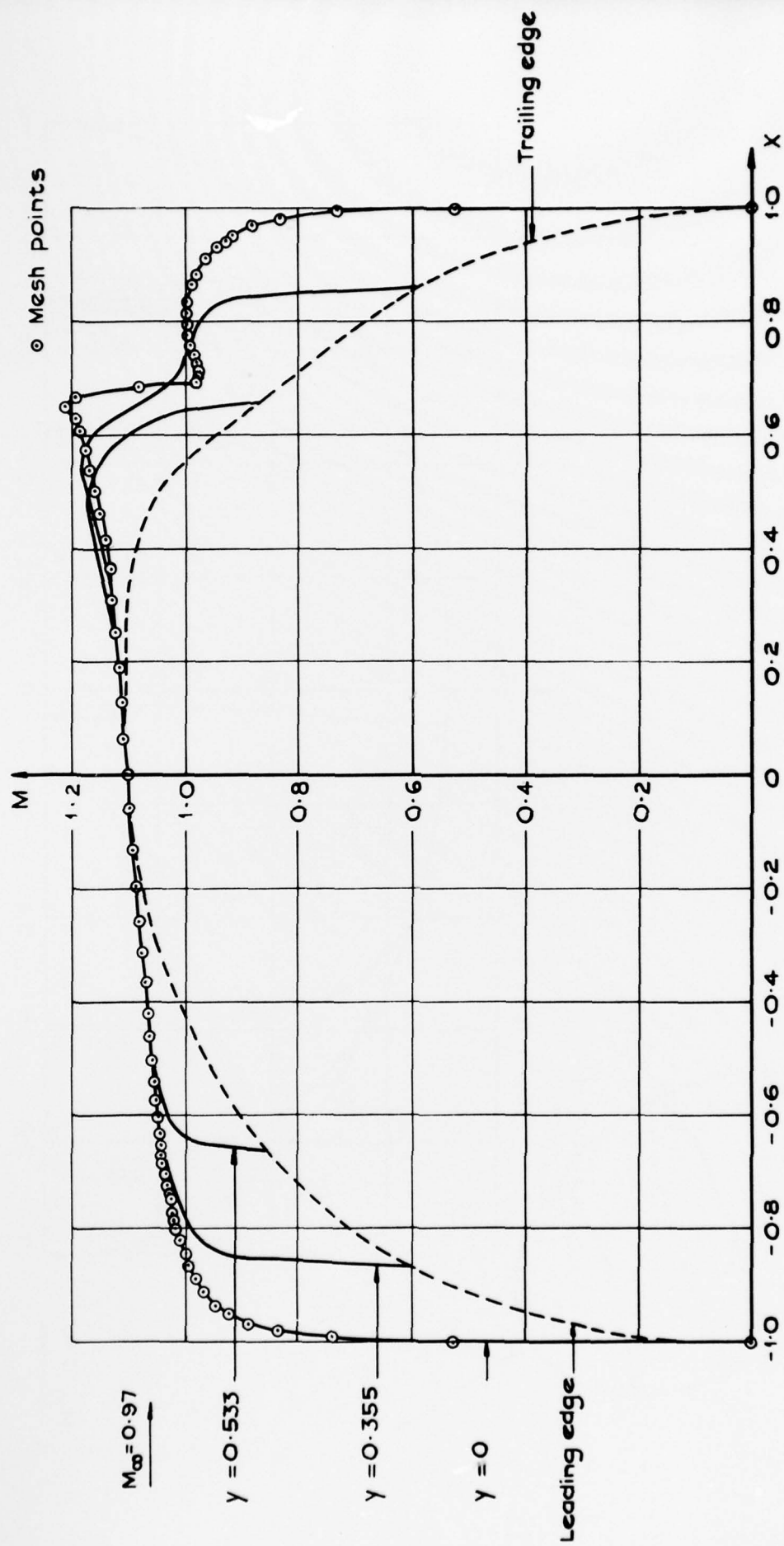


FIG. 13. Mach number distributions along lines  $y = \text{constant}$  on body surface  $M_\infty = 0.97$   $\Phi_\infty = x$  Body I.

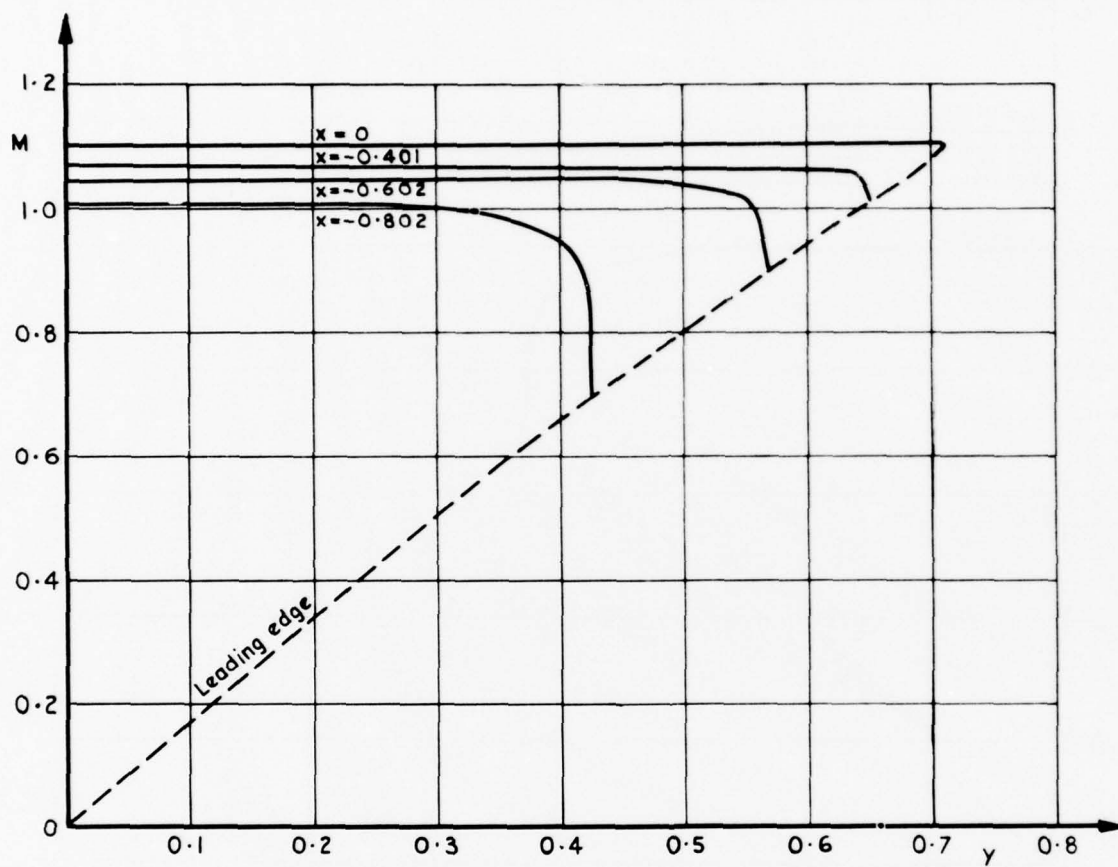


FIG. 14. Mach number distributions along lines  $x = \text{constant}$  on body surface ( $x \leq 0$ )  $M_\infty = 0.97$   $\Phi_\infty = x$  Body I.

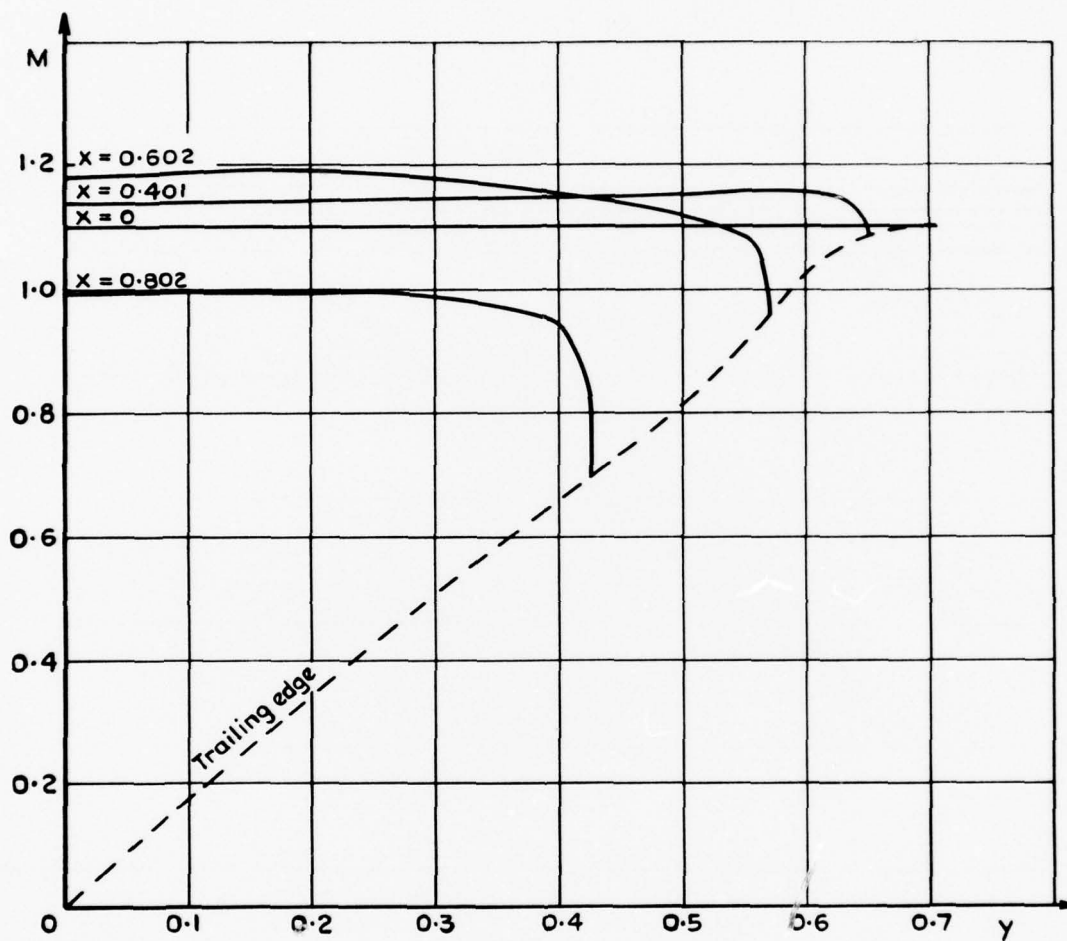


FIG. 15. Mach number distributions along lines  $x = \text{constant}$  on body surface ( $x \geq 0$ )  $M_\infty = 0.97$   $\Phi_\infty = x$   
Body I.

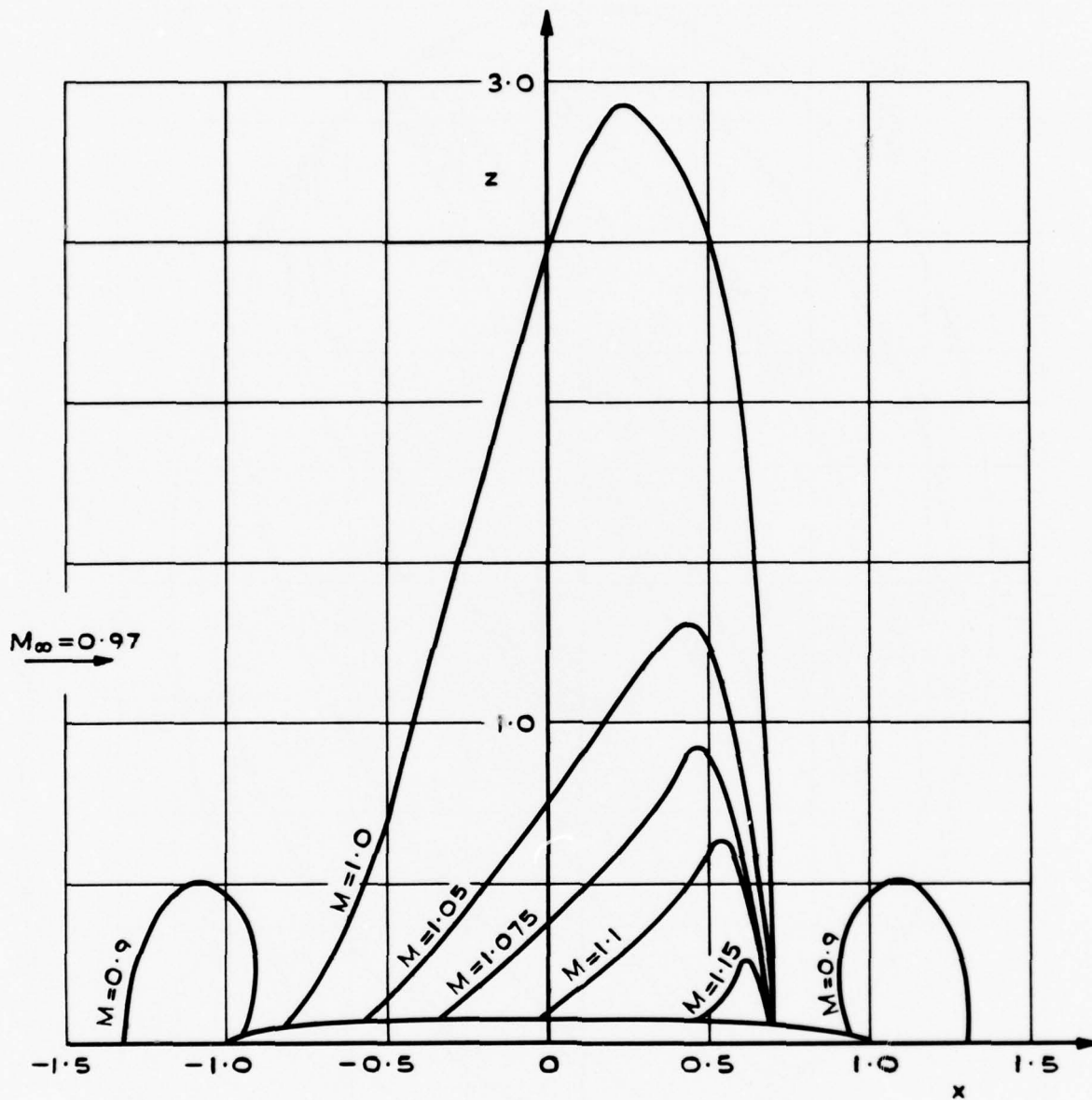


FIG. 16. Lines of constant Mach number in the plane  $y = 0$   $M_\infty = 0.97$   $\Phi_\infty = y$  Body I.

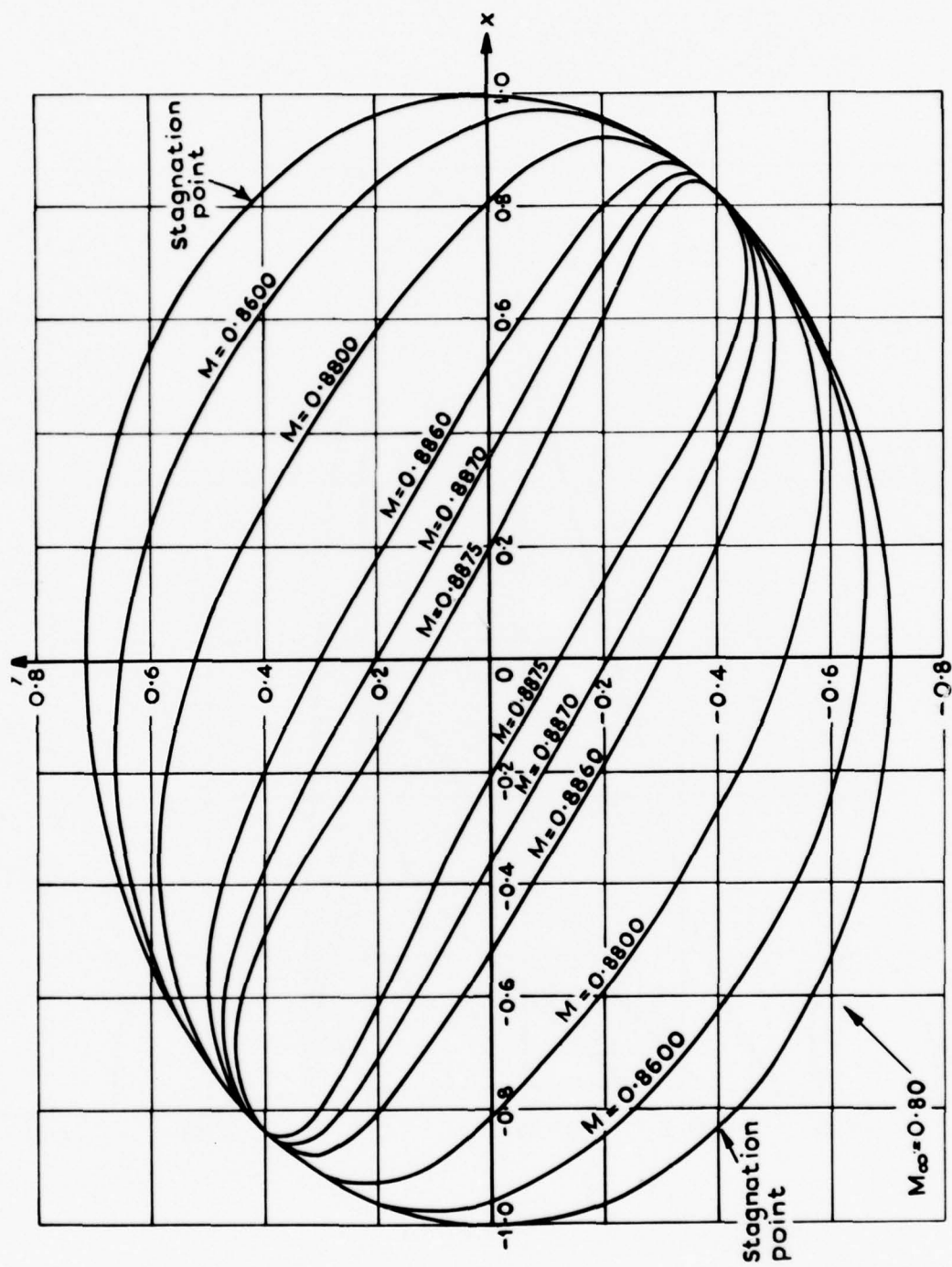


FIG. 17. Lines of constant Mach number on body surface  $M_\infty = 0.80$   $\Phi_x = (1/\sqrt{2})(x+y)$  Body I.

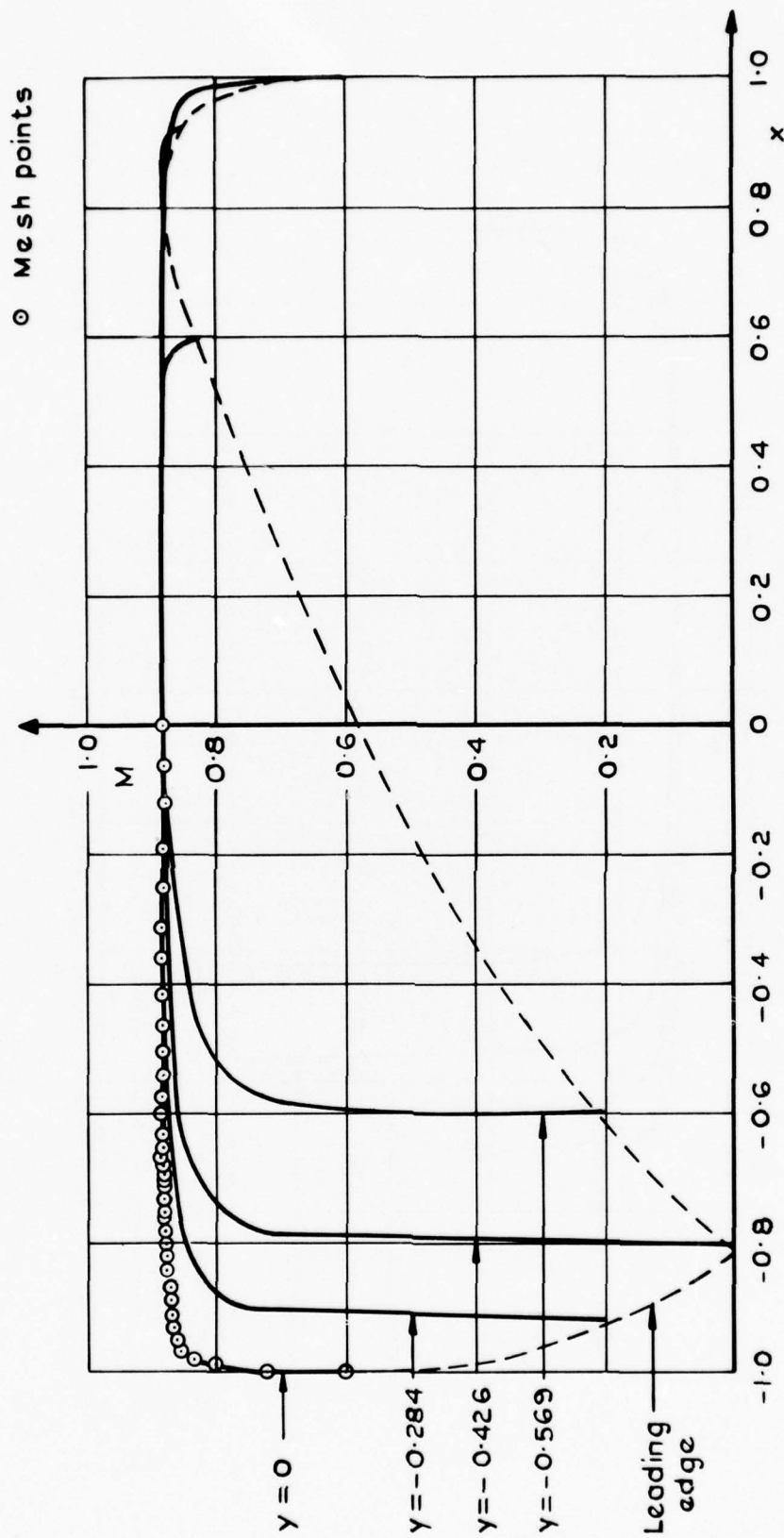


FIG. 18. Mach number distributions along lines  $y = \text{constant}$  on body surface  $M_{\infty} = 0.80$   $\Phi_{\infty} = (1/\sqrt{2})(x + y)$  Body I.

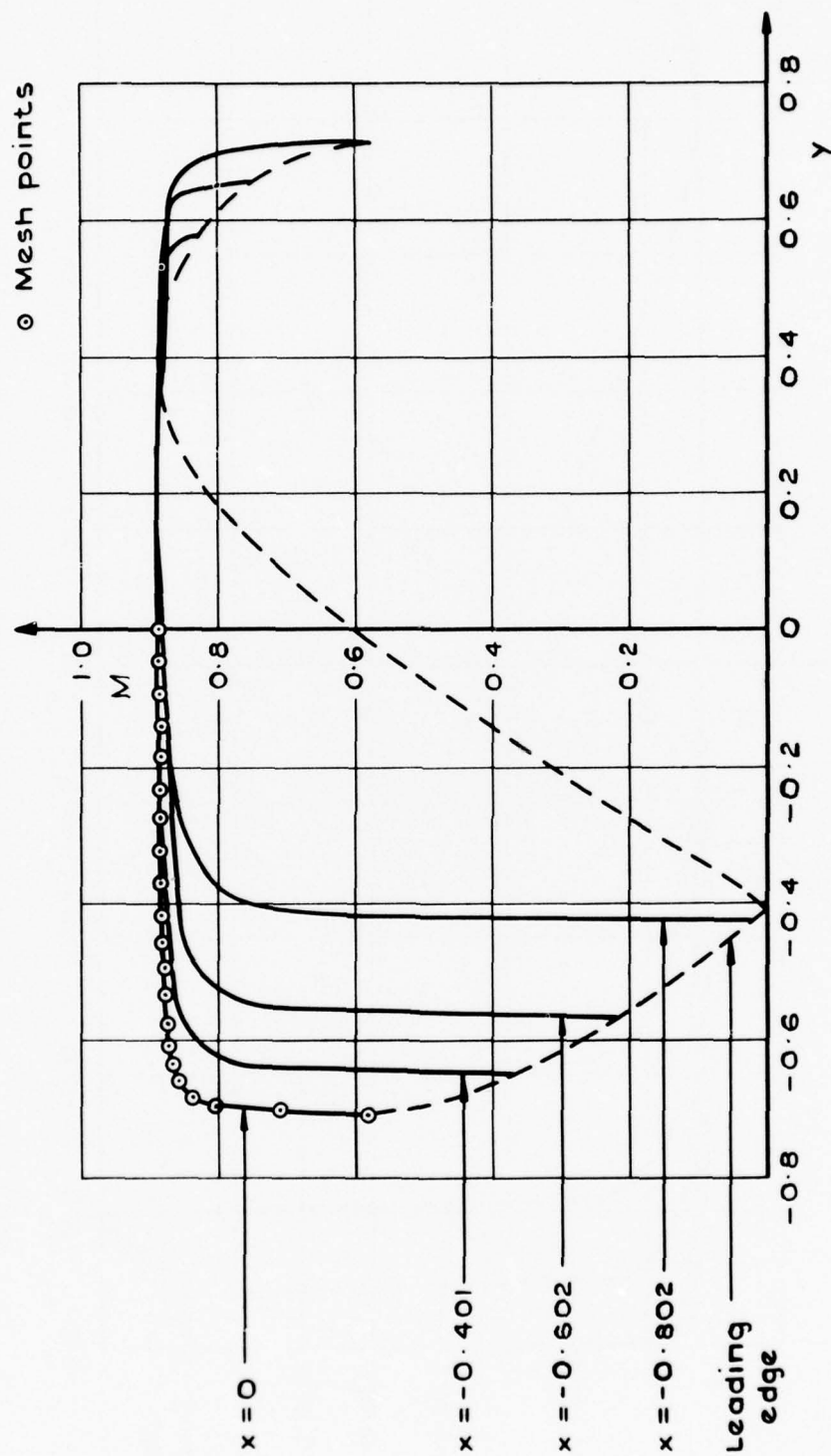


FIG. 19. Mach number distributions along lines  $x = \text{constant}$  on body surface  $M_x = 0.80$   $\Phi_x = (1/\sqrt{2})(x+y)$  Body I.

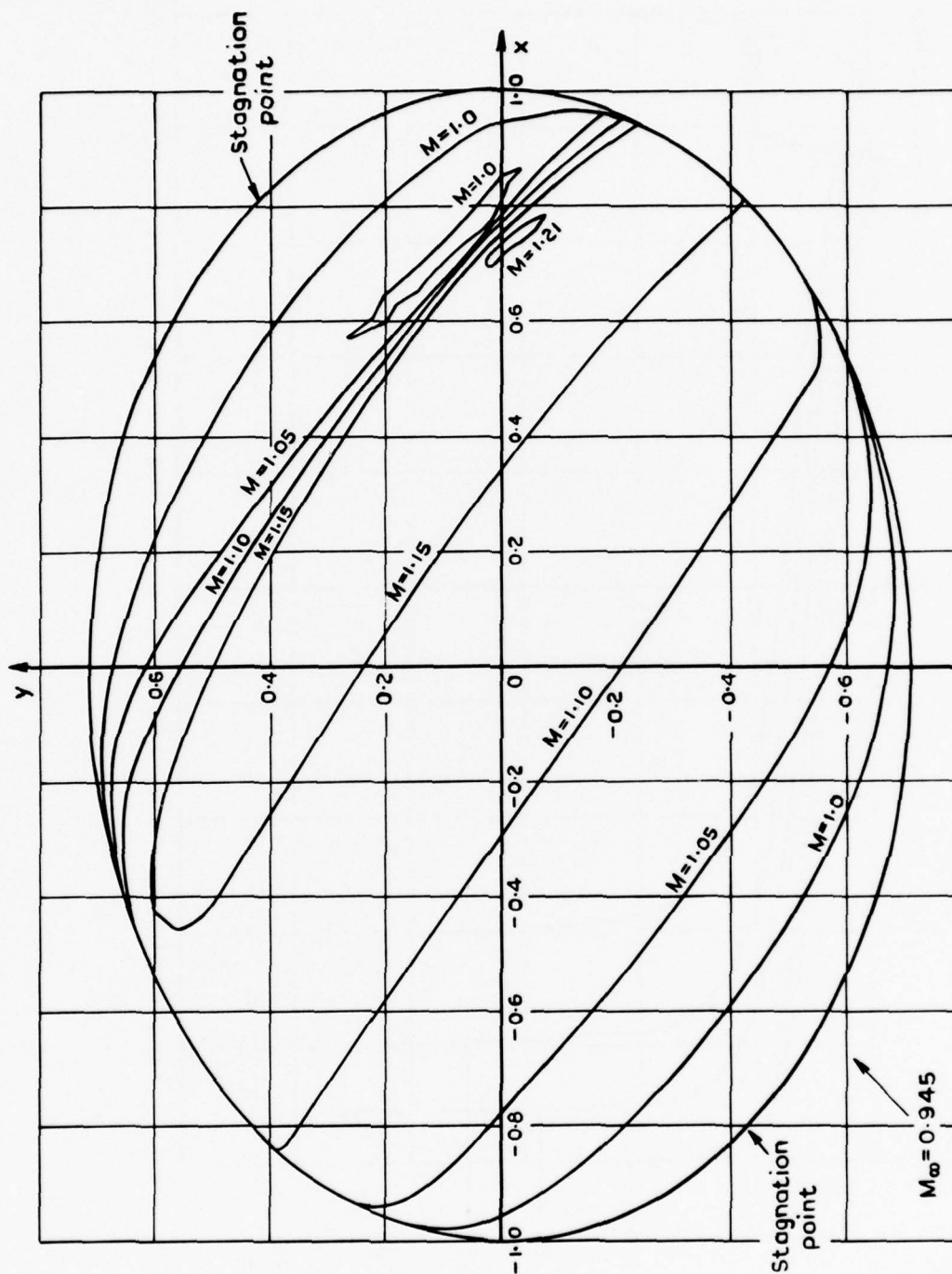


FIG. 20. Lines of constant Mach number on body surface  $M_\infty = 0.945 \Phi_x = 1/\sqrt{2}(x+y)$  Body I.

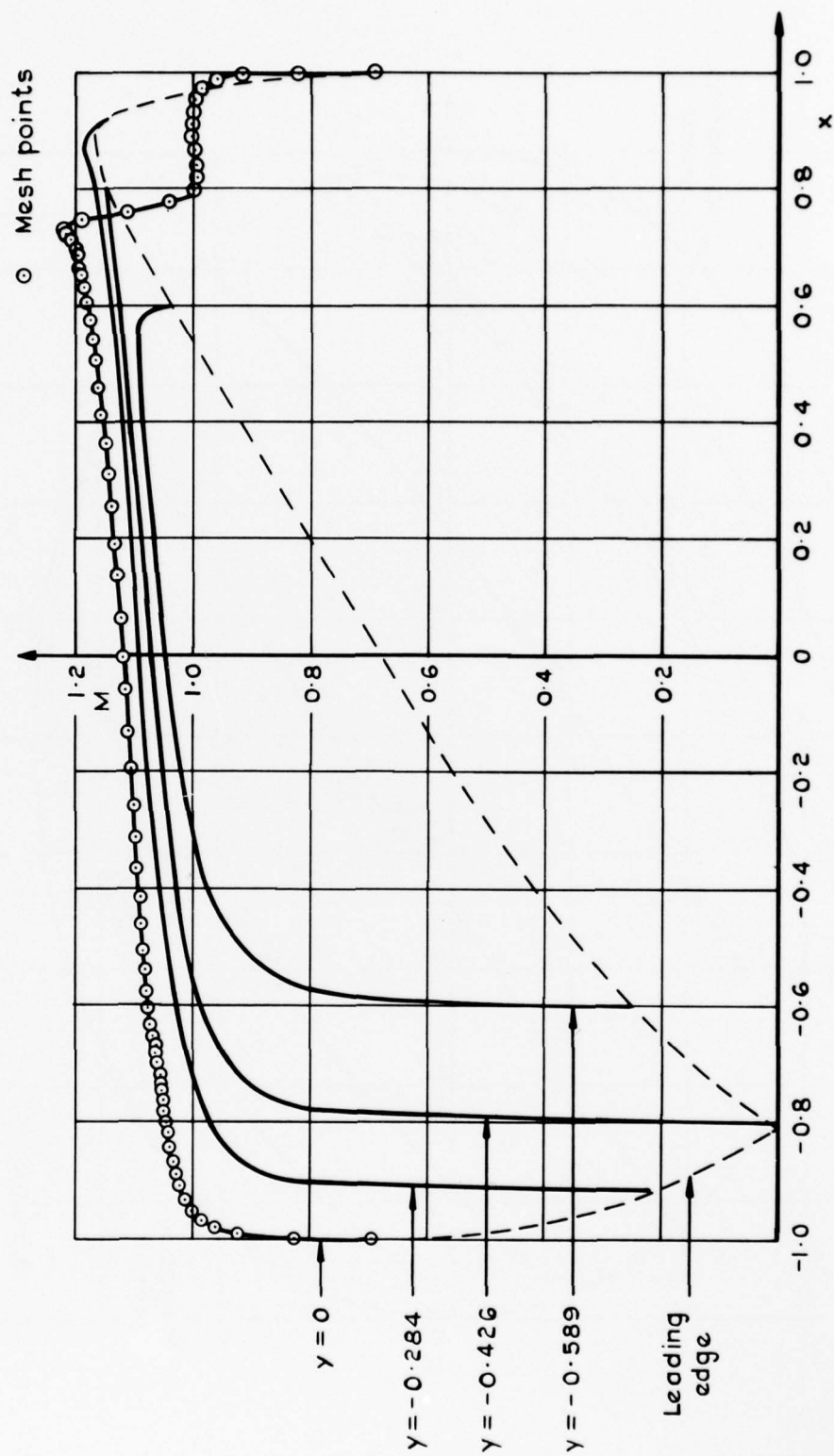


FIG. 21. Mach number distributions along lines  $y = \text{constant}$  on body surface ( $y \leq 0$ )  $M_{\infty} = 0.945$   $\Phi_x = (1/\sqrt{2})(x + y)$  Body I.

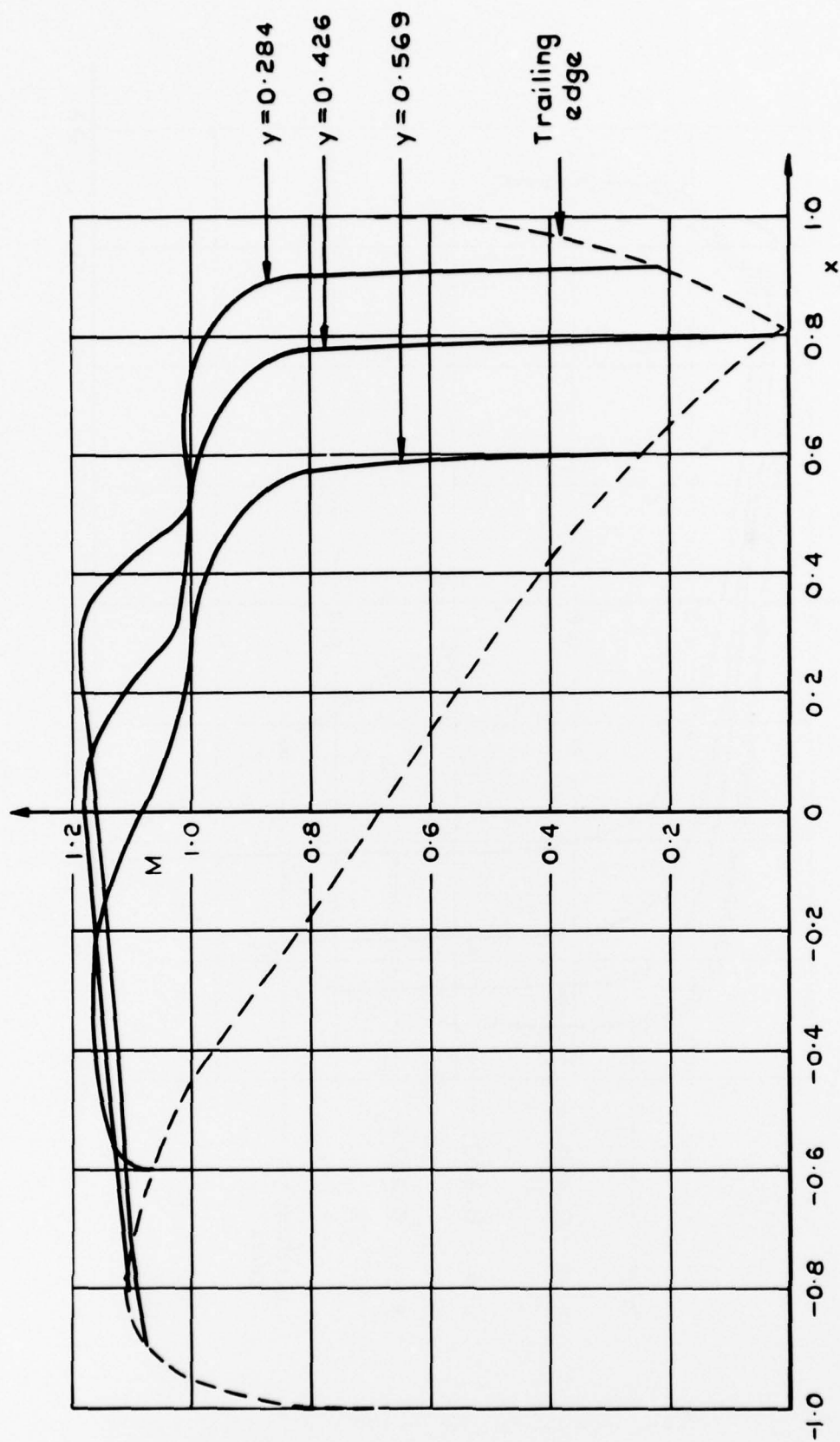


FIG. 22. Mach number distributions along lines  $y = \text{constant}$  on body surface ( $y > 0$ )  $M_\infty = 0.945$   $\Phi_\infty = (1/\sqrt{2})(x + y)$  Body I.

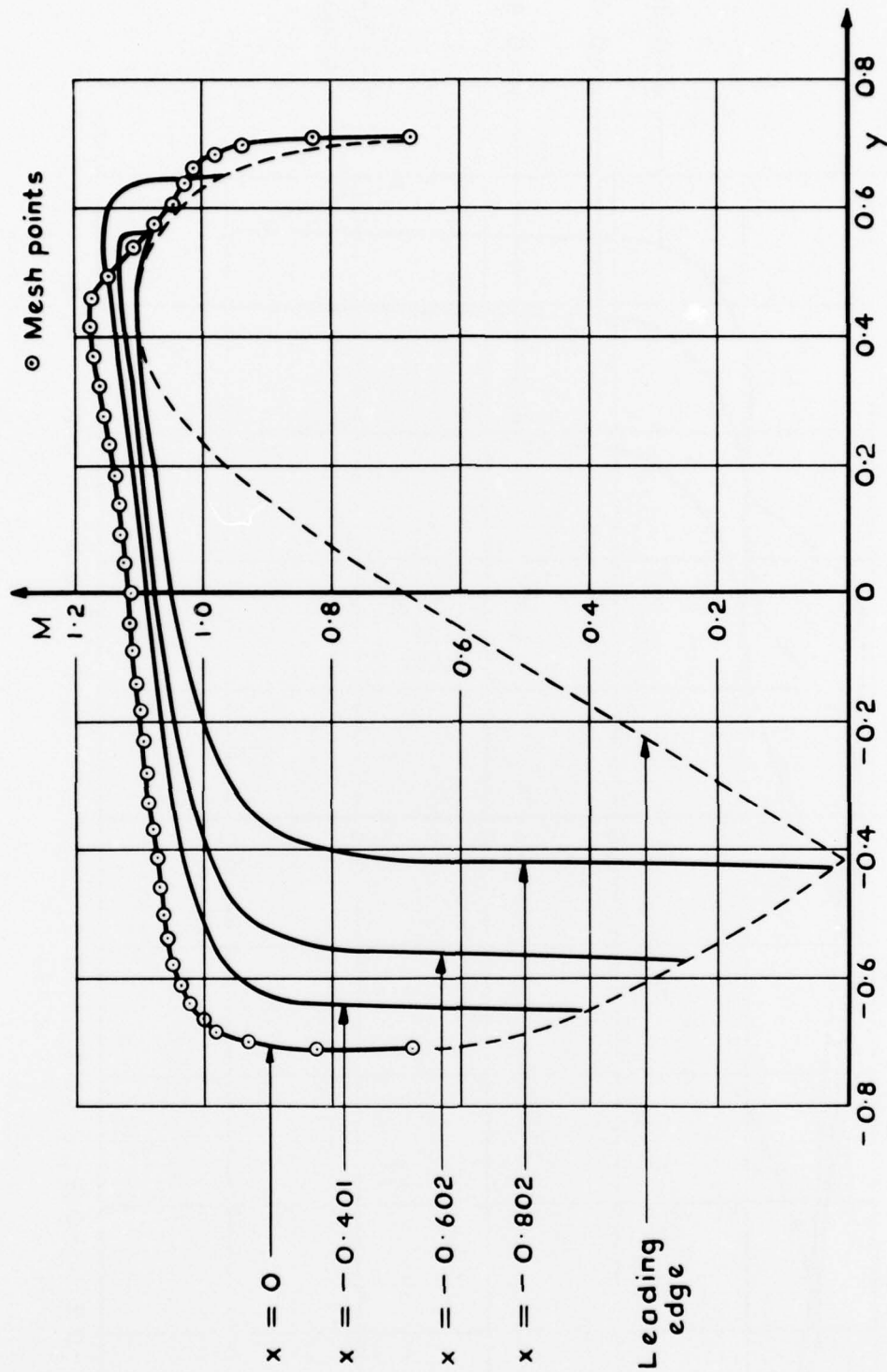


FIG. 23. Mach number distributions along lines  $x = \text{constant}$  on body surface ( $x \leq 0$ )  $M_\infty = 0.945$   $\Phi_\infty = (1/\sqrt{2})(x+y)$  Body I.

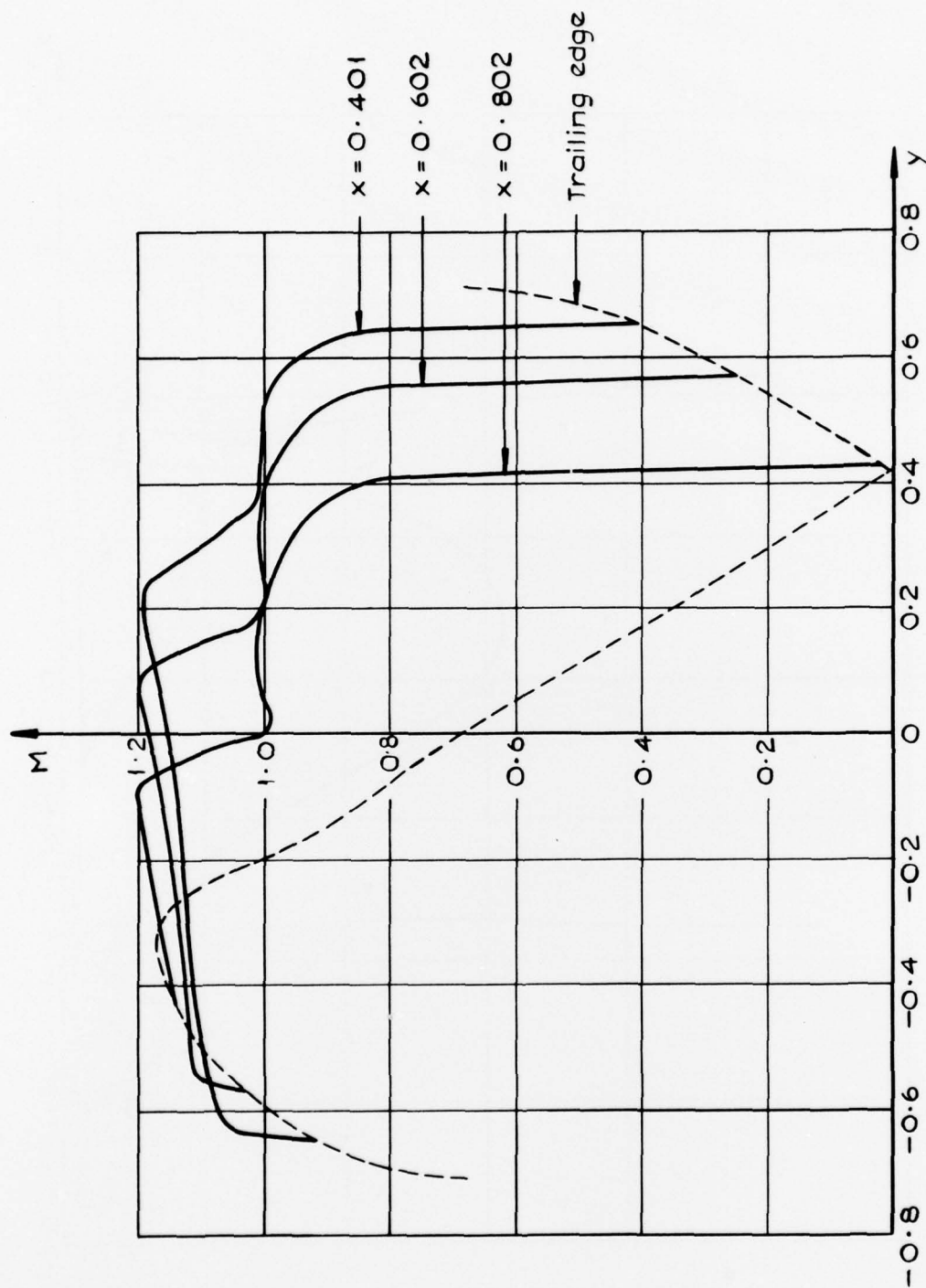


FIG. 24. Mach number distributions along lines  $x = \text{constant}$  on body surface ( $x > 0$ )  $M_\infty = 0.945$   $\Phi_\infty = (1/\sqrt{2})(x+y)$  Body I.

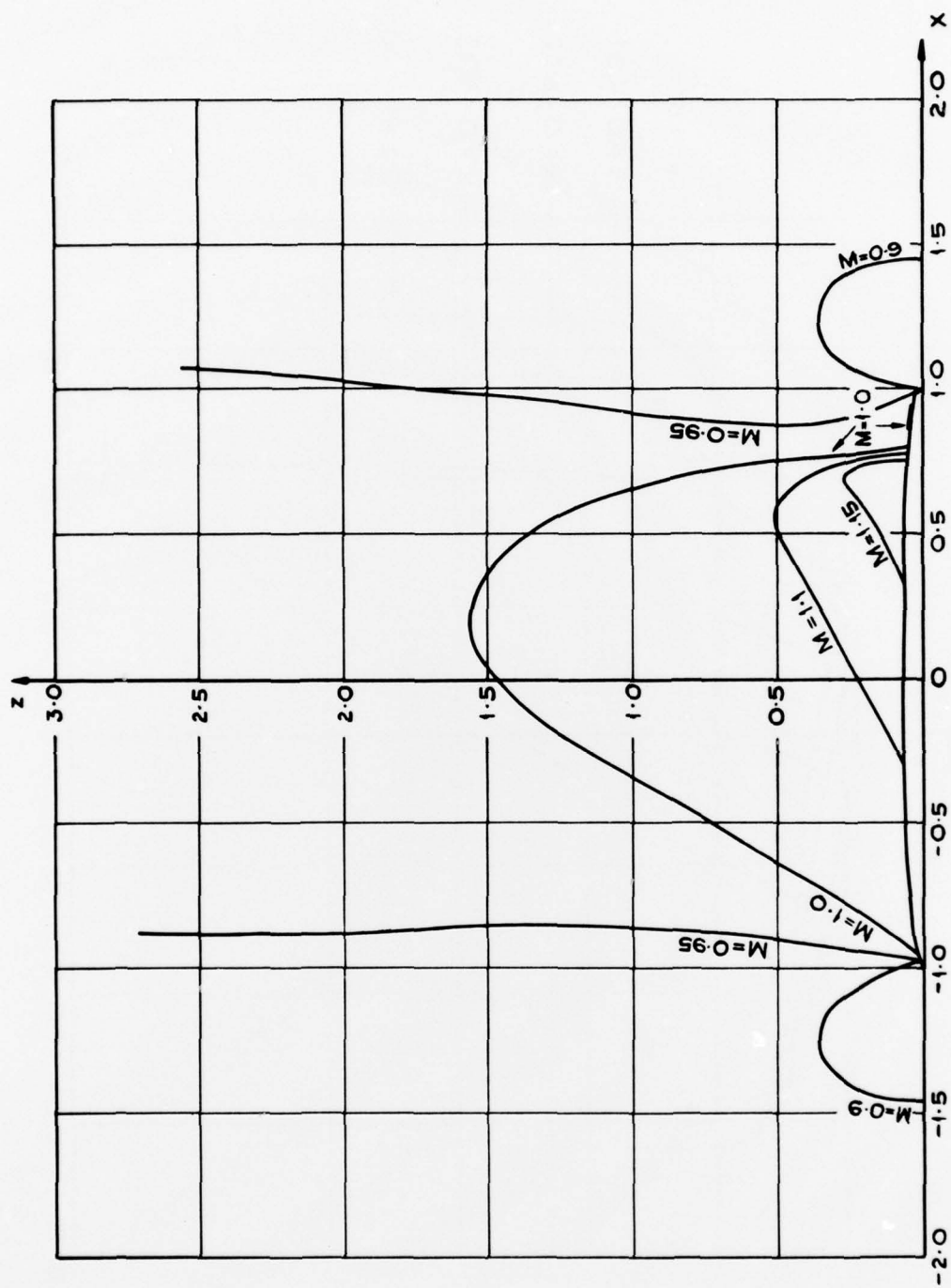


FIG. 25. Lines of constant Mach number in the plane  $y = 0$   $M_{\infty} = 0.945$   $\Phi_x = (1/\sqrt{2})(x+y)$  Body I.

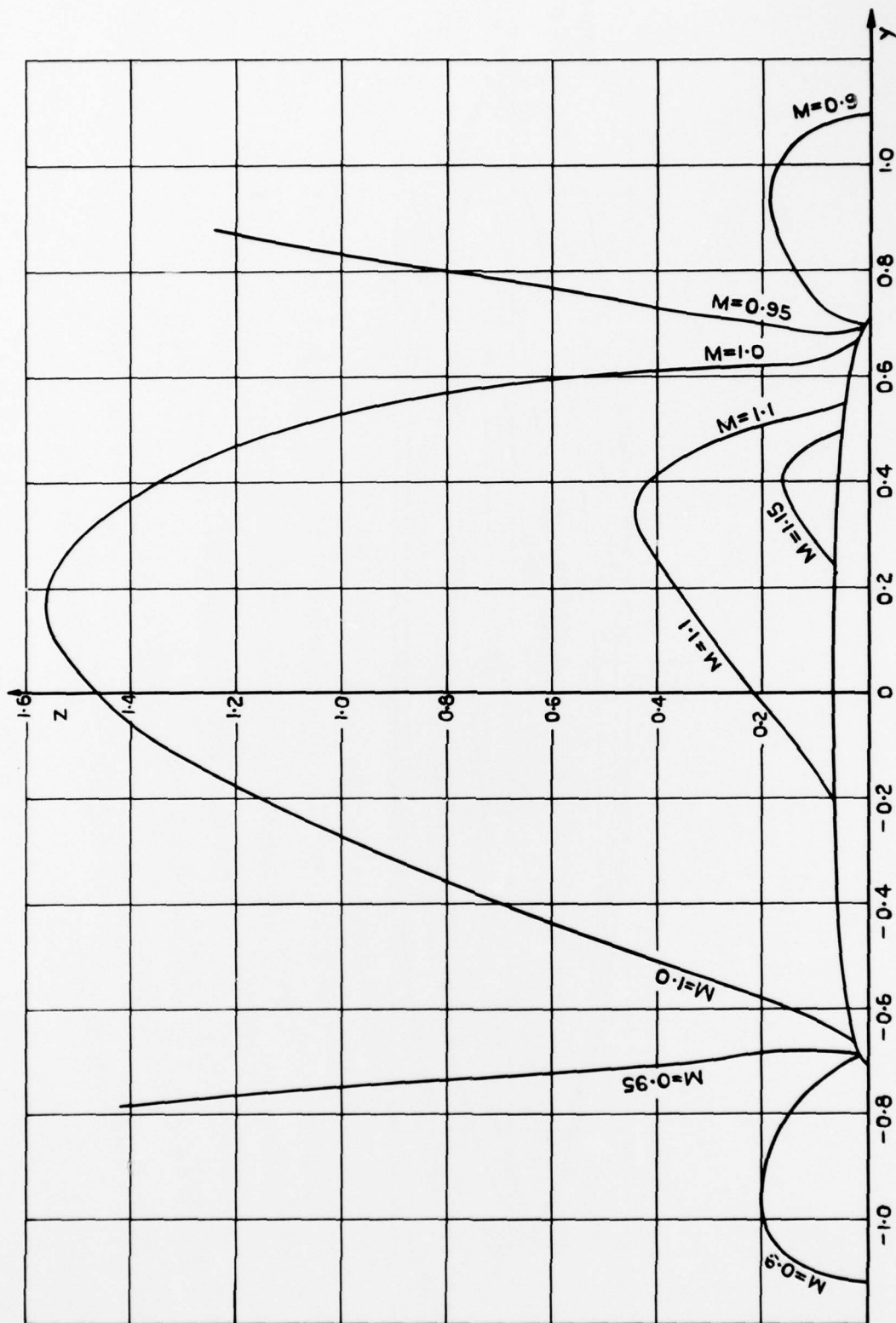


FIG. 26. Lines of constant Mach number in the plane  $x = 0$   $M_{\infty} = 0.945$   $\Phi_{\infty} = (1/\sqrt{2})(x+y)$  Body I.

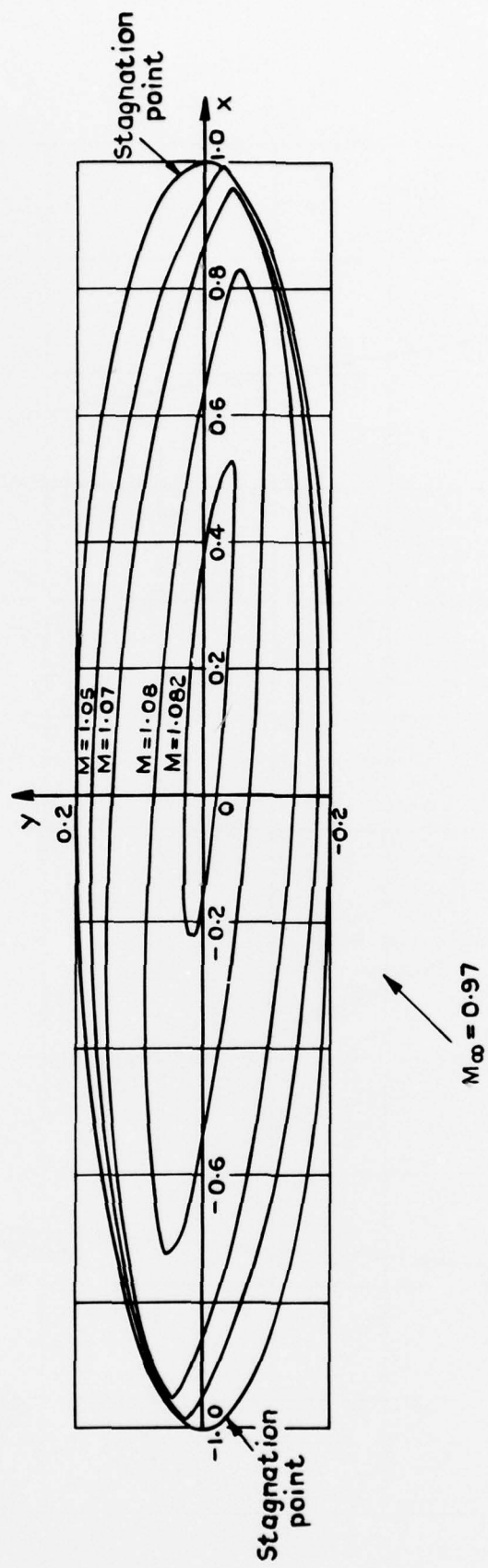


FIG. 27. Lines of constant Mach number on body surface  $M_{\infty} = 0.97$   $\Phi_{\infty} = (1/\sqrt{2})(x+y)$  Body II.

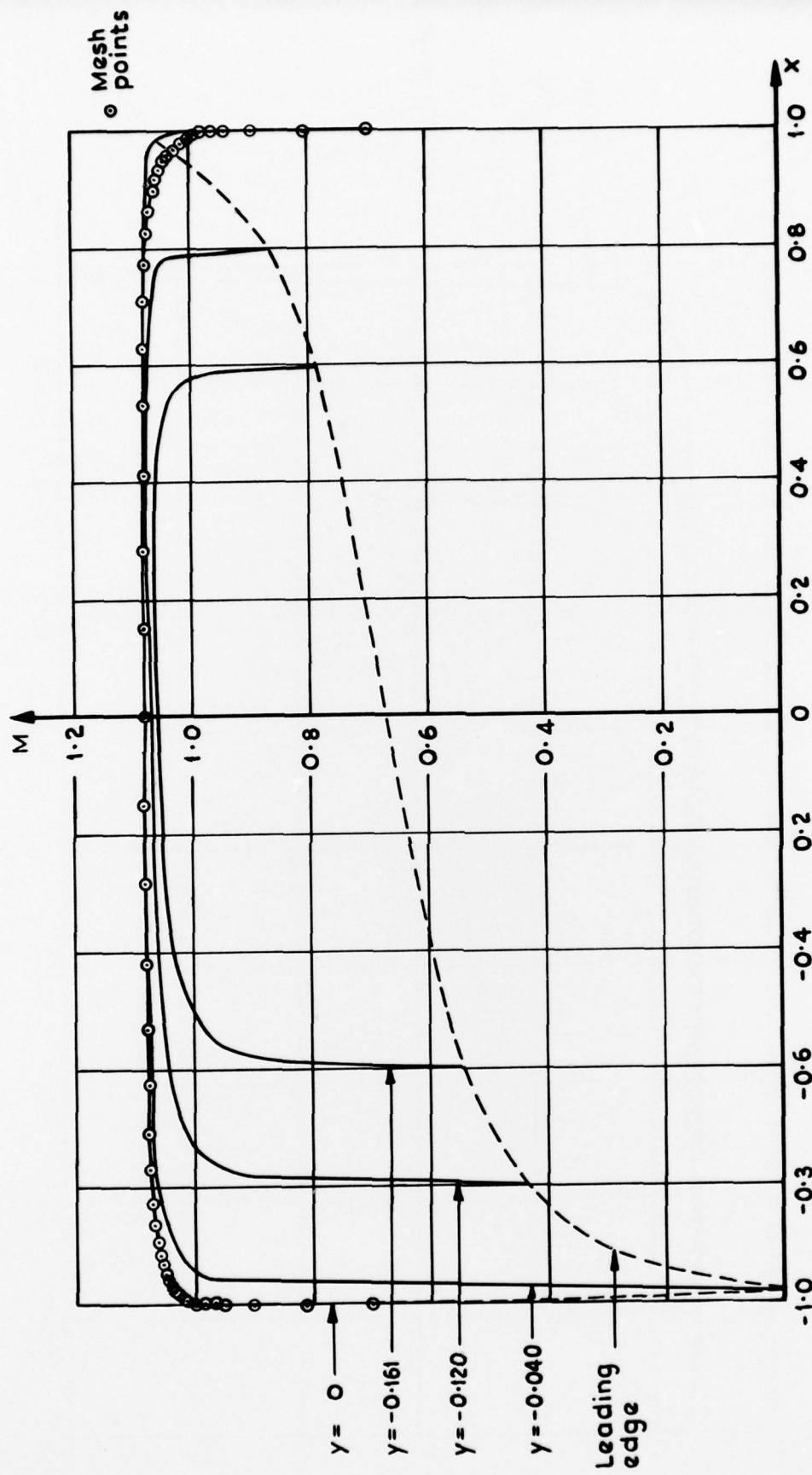


FIG. 28. Mach number distributions along lines  $y = \text{constant}$  on body surface ( $y \leq 0$ )  $M_\infty = 0.97$   $\Phi = (1/\sqrt{2})(x + y)$  Body II.

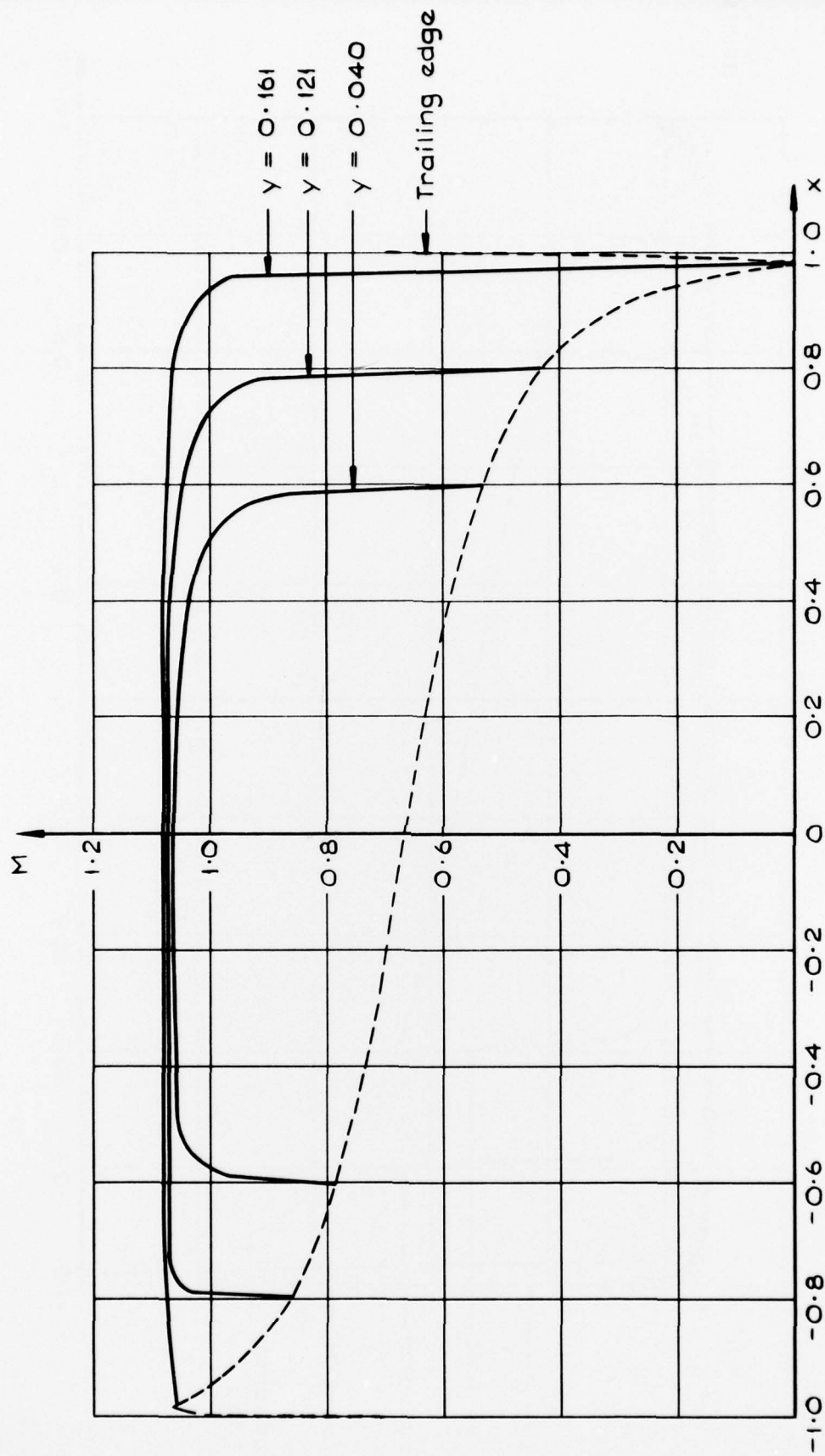


FIG. 29. Mach number distributions along lines  $y = \text{constant}$  on body surface ( $y > 0$ )  $M_x = 0.97$   $\Phi_x = (1/\sqrt{2})(x + y)$  Body II.

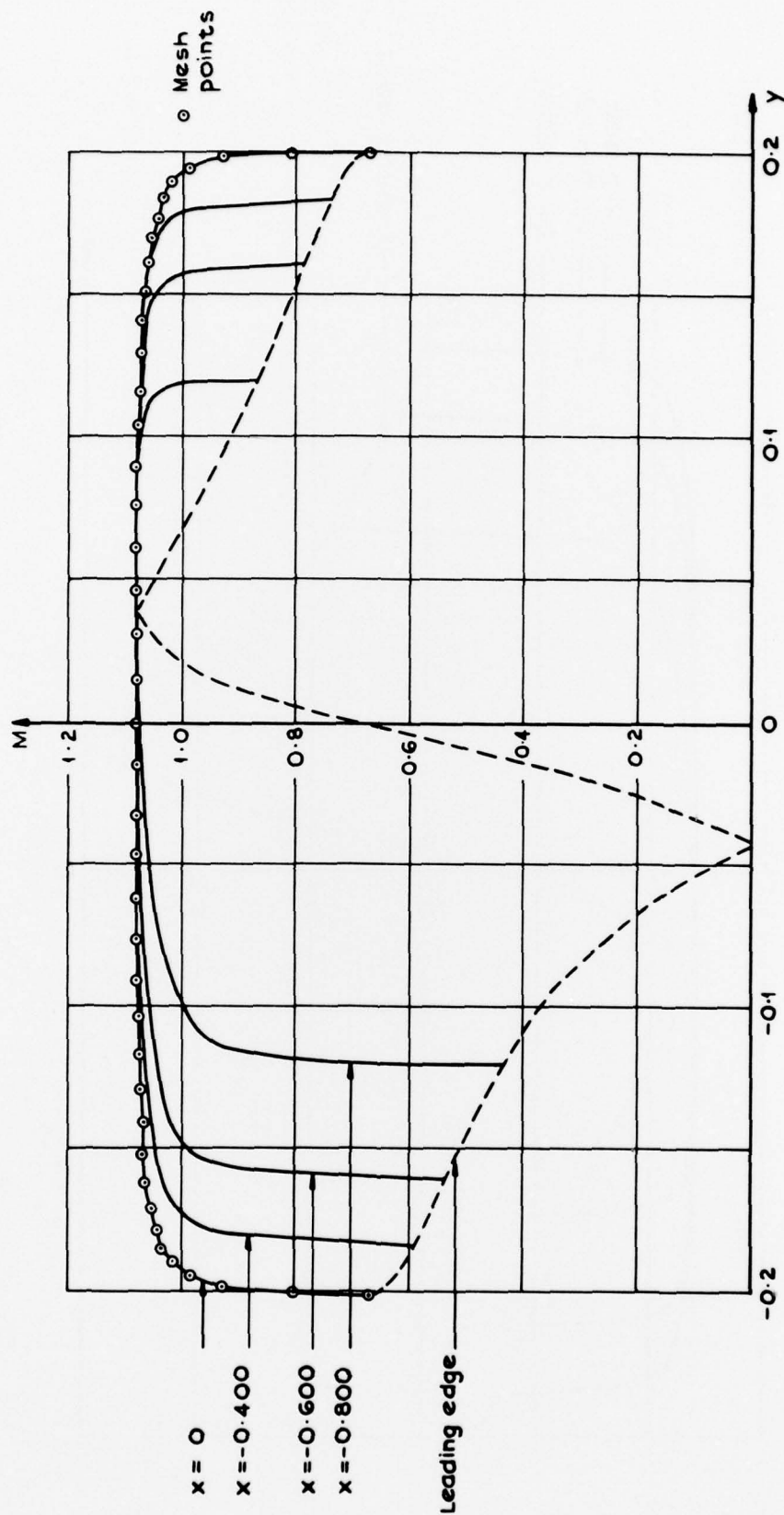


FIG. 30. Mach number distributions along lines  $x = \text{constant}$  on body surface ( $x \leq 0$ )  $M_\infty = 0.97 \Phi_\infty = (1/\sqrt{2})(x+y)$  Body II.

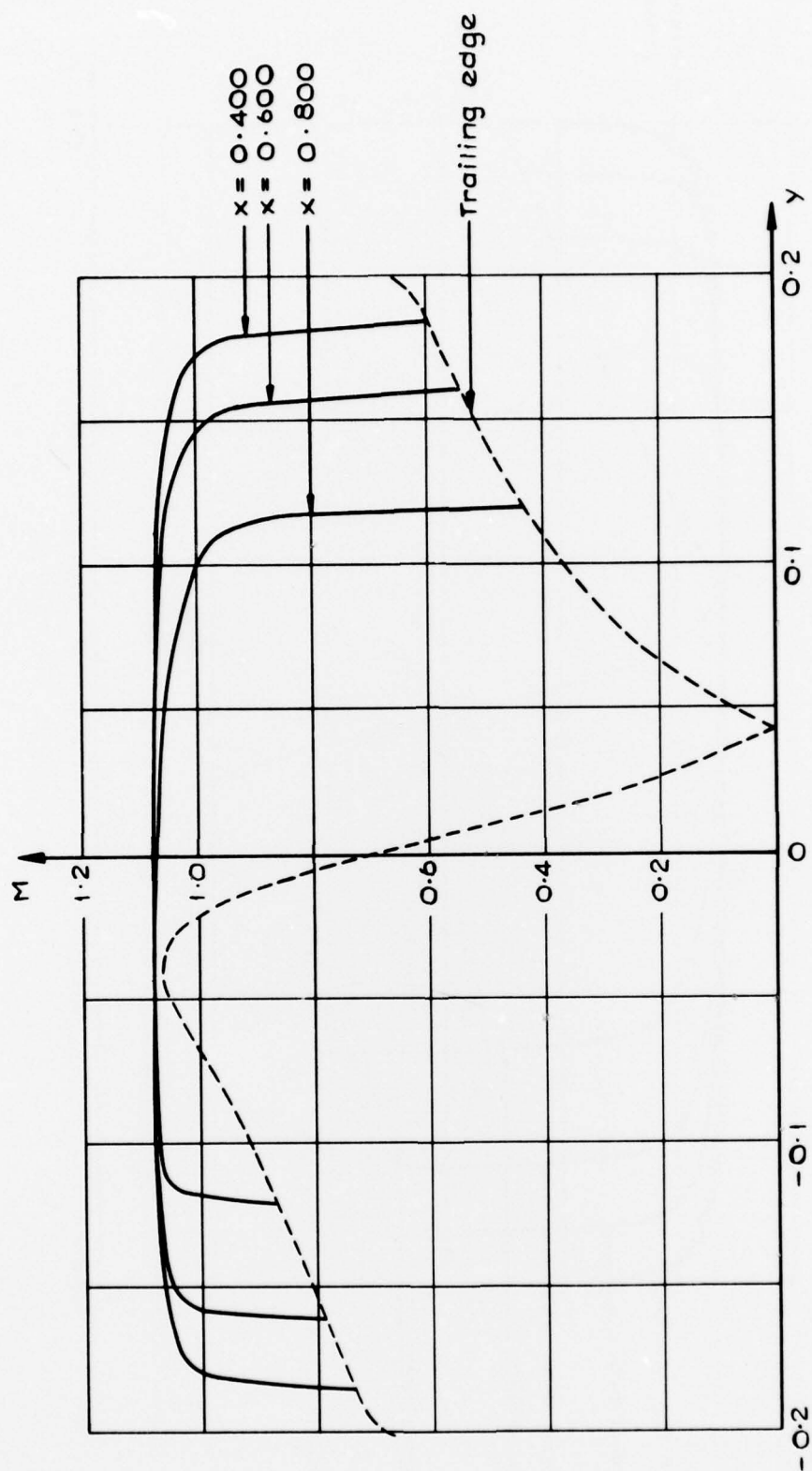


FIG. 31. Mach number distributions along lines  $x = \text{constant}$  on body surface ( $x > 0$ )  $M_{\infty} = 0.97$   $\Phi_{\infty} = (1/\sqrt{2})(x+y)$  Body II.

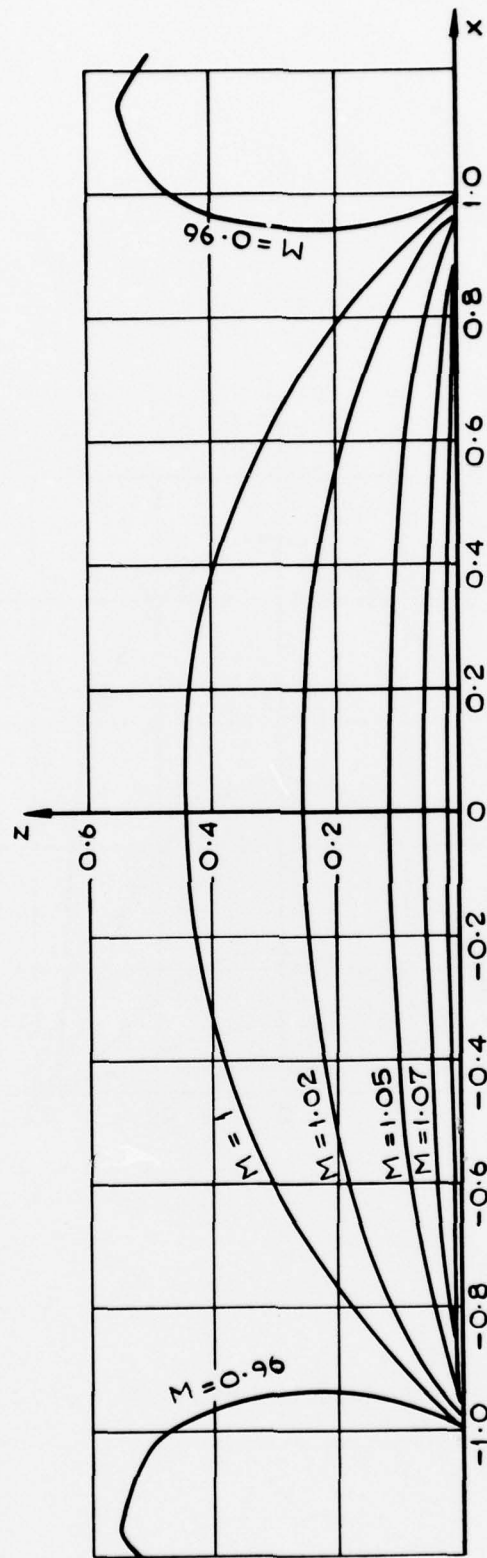


FIG. 32. Lines of constant Mach number in the plane  $y = 0$   $M_x = 0.97$   $\Phi_x = (1/\sqrt{2})(x + y)$  Body II.

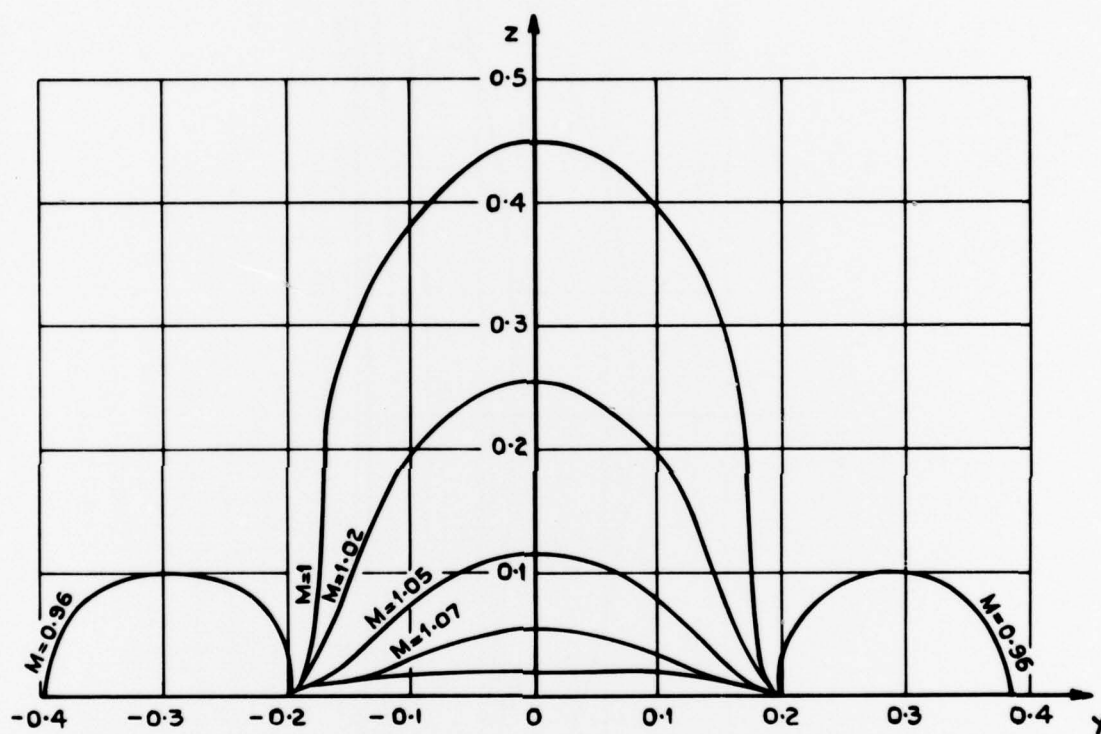


FIG. 33. Lines of constant Mach number in the plane  $x = 0$   $M_{\infty} = 0.97$   $\Phi_{\infty} = (1/\sqrt{2})(x + y)$  Body II.

**A.R.C. R. & M. No. 3794**  
August, 1975  
P. W. Duck

THE NUMERICAL CALCULATION OF  
STEADY INVISCID SUPERCritical FLOW PAST  
ELLIPSOIDS WITHOUT CIRCULATION

The previous work of the author in which the supercritical flow past ellipsoids was calculated is extended to supercritical flows. The same ellipsoidal coordinate system is used, the body-surface boundary-condition is then applied exactly (in the numerical sense). By means of a transformation of one of the coordinates, the infinite flow field is brought into a finite space for the calculation.

The complete continuity equation is approximated by the usual central differencing in the elliptic (subcritical) regions, whilst in the

**A.R.C. R. & M. No. 3794**  
August, 1975  
P. W. Duck

THE NUMERICAL CALCULATION OF  
STEADY INVISCID SUPERCritical FLOW PAST  
ELLIPSOIDS WITHOUT CIRCULATION

The previous work of the author in which the supercritical flow past ellipsoids was calculated is extended to supercritical flows. The same ellipsoidal coordinate system is used, the body-surface boundary-condition is then applied exactly (in the numerical sense). By means of a transformation of one of the coordinates, the infinite flow field is brought into a finite space for the calculation.

The complete continuity equation is approximated by the usual central differencing in the elliptic (subcritical) regions, whilst in the

**A.R.C. R. & M. No. 3794**  
August, 1975  
P. W. Duck

THE NUMERICAL CALCULATION OF  
STEADY INVISCID SUPERCritical FLOW PAST  
ELLIPSOIDS WITHOUT CIRCULATION

The previous work of the author in which the supercritical flow past ellipsoids was calculated is extended to supercritical flows. The same ellipsoidal coordinate system is used, the body-surface boundary-condition is then applied exactly (in the numerical sense). By means of a transformation of one of the coordinates, the infinite flow field is brought into a finite space for the calculation.

The complete continuity equation is approximated by the usual central differencing in the elliptic (subcritical) regions, whilst in the

**A.R.C. R. & M. No. 3794**  
August, 1975  
P. W. Duck

THE NUMERICAL CALCULATION OF  
STEADY INVISCID SUPERCritical FLOW PAST  
ELLIPSOIDS WITHOUT CIRCULATION

The previous work of the author in which the supercritical flow past ellipsoids was calculated is extended to supercritical flows. The same ellipsoidal coordinate system is used, the body-surface boundary-condition is then applied exactly (in the numerical sense). By means of a transformation of one of the coordinates, the infinite flow field is brought into a finite space for the calculation.

The complete continuity equation is approximated by the usual central differencing in the elliptic (subcritical) regions, whilst in the

hyperbolic (supercritical) regions, the combination of central and non-central differencing as suggested by Albone and Jameson is used, in order to model the absence of upstream propagation of disturbances.

Although shock waves appear in the calculations, their shape and position is only approximately determined (as *e.g.* in transonic small perturbation theory) since the difference scheme only ensures continuity of the potential across the shock, the Rankine-Hugoniot equations not being satisfied. A number of results is presented, for flows aligned along the major and second major axes, and also yawed relative to these two axes.

hyperbolic (supercritical) regions, the combination of central and non-central differencing as suggested by Albone and Jameson is used, in order to model the absence of upstream propagation of disturbances.

Although shock waves appear in the calculations, their shape and position is only approximately determined (as *e.g.* in transonic small perturbation theory) since the difference scheme only ensures continuity of the potential across the shock, the Rankine-Hugoniot equations not being satisfied. A number of results is presented, for flows aligned along the major and second major axes, and also yawed relative to these two axes.

hyperbolic (supercritical) regions, the combination of central and non-central differencing as suggested by Albone and Jameson is used, in order to model the absence of upstream propagation of disturbances.

Although shock waves appear in the calculations, their shape and position is only approximately determined (as *e.g.* in transonic small perturbation theory) since the difference scheme only ensures continuity of the potential across the shock, the Rankine-Hugoniot equations not being satisfied. A number of results is presented, for flows aligned along the major and second major axes, and also yawed relative to these two axes.

hyperbolic (supercritical) regions, the combination of central and non-central differencing as suggested by Albone and Jameson is used, in order to model the absence of upstream propagation of disturbances.

Although shock waves appear in the calculations, their shape and position is only approximately determined (as *e.g.* in transonic small perturbation theory) since the difference scheme only ensures continuity of the potential across the shock, the Rankine-Hugoniot equations not being satisfied. A number of results is presented, for flows aligned along the major and second major axes, and also yawed relative to these two axes.